

CHAPTER 7

Figures

These figures are from

Understanding the properties of matter

by Michael de Podesta.

The copyright of these figures resides with the publishers, *Taylor and Francis*.

The figures may be used freely for educational purposes, but their source must be acknowledged.

For more details see www.physicsofmatter.com

Figure 7.1 The densities of the elements plotted against atomic number, i.e. the number of electrons on each atom. A great deal of structure is evident. The troughs *a*, *b*, *c*, *d* occur just after the completion of the main electron shells of the atoms; *a* = K (Potassium); *b* = Rb (Rubidium); *c* = Cs (Caesium); *d* = Fr (Francium). The peaks *e*, *f*, and *g* are between the middle and end of the filling of the *d* - electron states in the three rows of *transition metals*; *e* = Zn (Zinc); *f* = Rh (Rhodium); *g* = Os (Osmium); the regular slope *h* represents the *Lanthanides*.

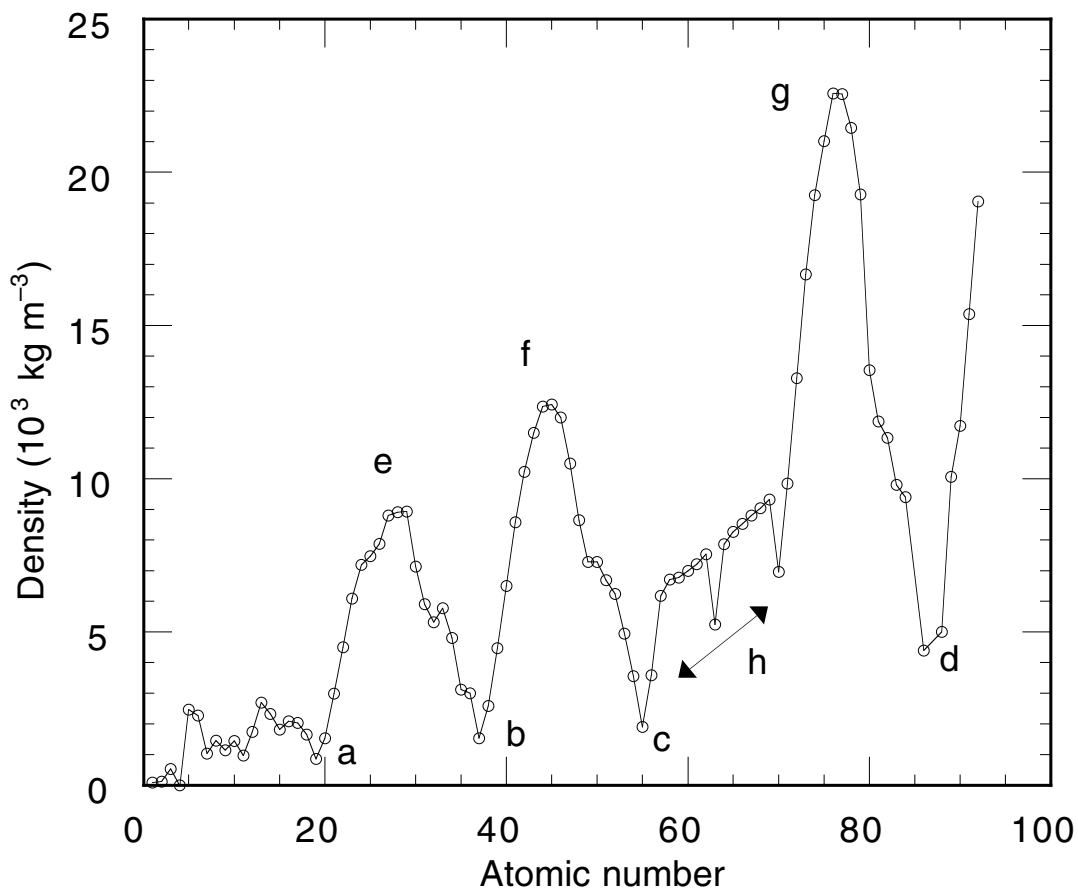


Figure 7.2 The densities of the elements plotted against atomic number. The solid line represents the expected density of the solid elements if they all had a simple cubic crystal structure with a nearest neighbour separation of 0.3 nm. (See Example 7.2)

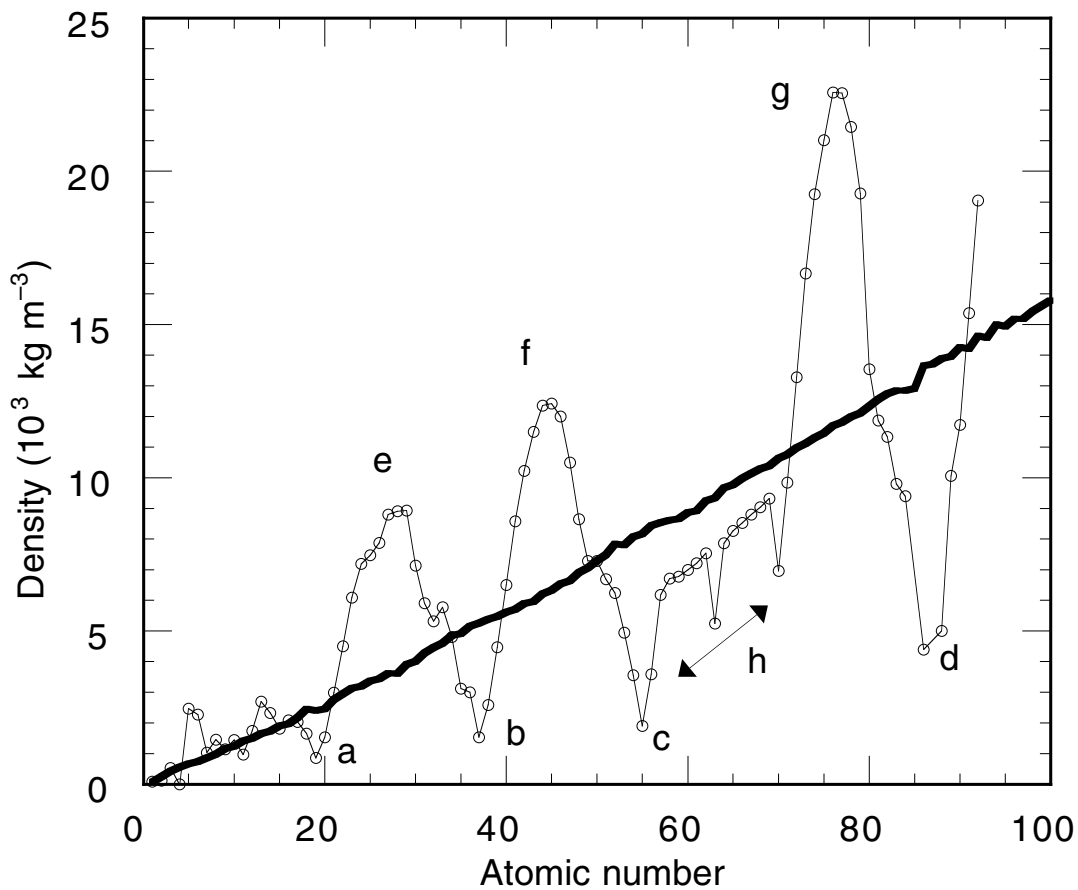
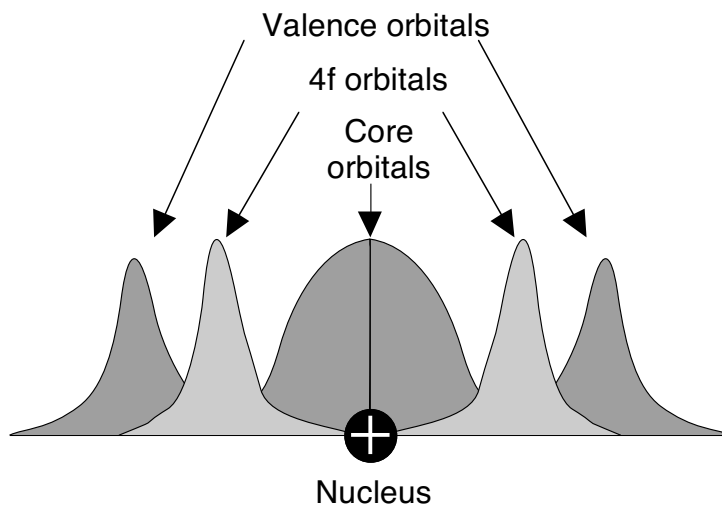
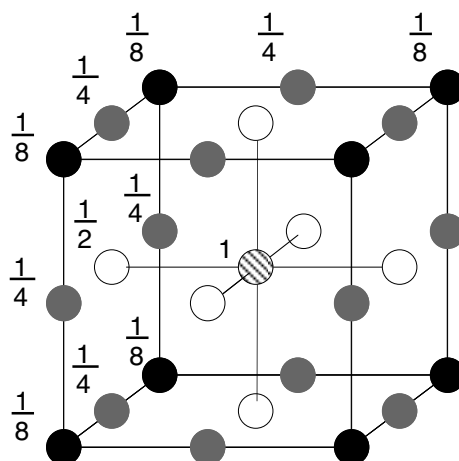
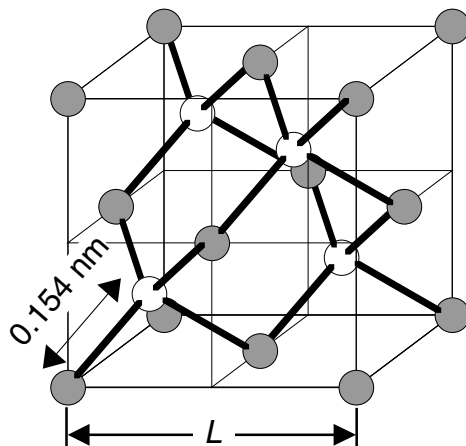


Figure 7.3 An entirely schematic diagram showing the location of the peak of the charge density associated with the 4f orbitals, and contrasting their position with that of the valence orbitals and the core orbitals.

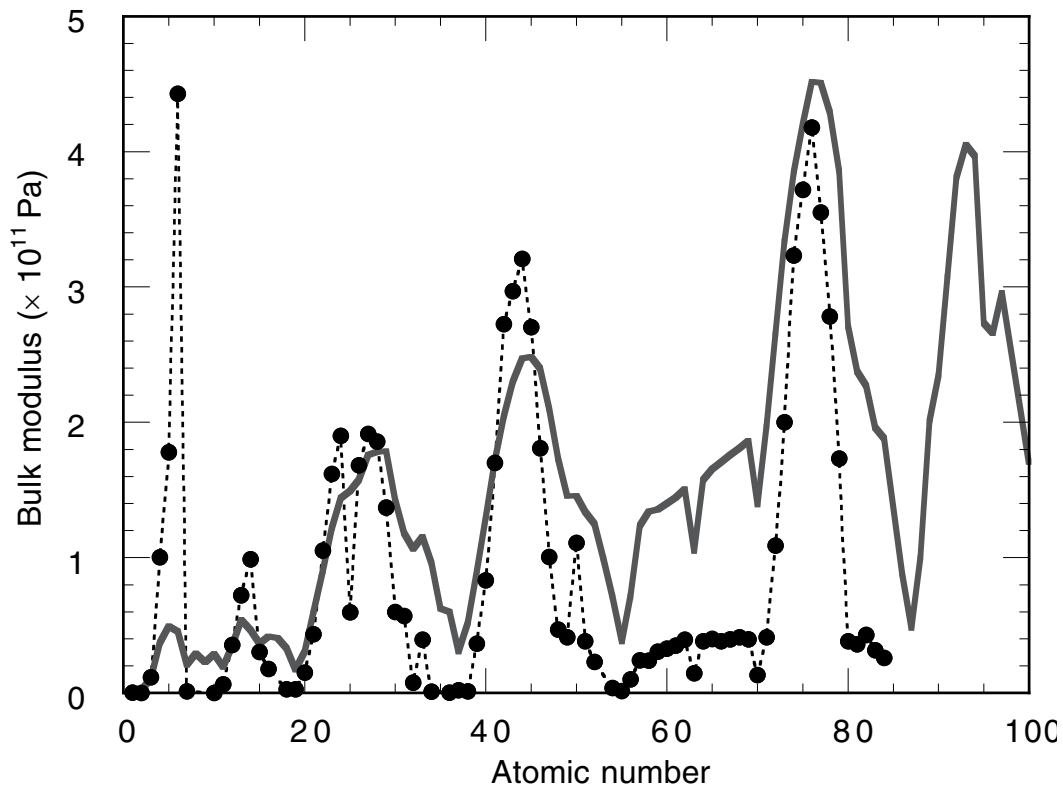


From Example 7.3



Extracted from *Understanding the properties of matter* by Michael de Podesta.
The copyright of these figures resides with Taylor and Francis.
They may be used freely for educational purposes but their source must be acknowledged.
For more details see www.physicsofmatter.com

Figure 7.4 The bulk modulus of the elements plotted as function of atomic number. Also shown as a grey continuous line (and on an arbitrary scale) is the density of the elements shown in Figure 7.1.



Extracted from *Understanding the properties of matter* by Michael de Podesta.
The copyright of these figures resides with *Taylor and Francis*.
They may be used freely for educational purposes but their source must be acknowledged.
For more details see www.physicsofmatter.com

Figure 7.5 (a) A pair potential curve and (b) its derivative. The bulk modulus is related to the slope of the first derivative at the point where the slope is zero.

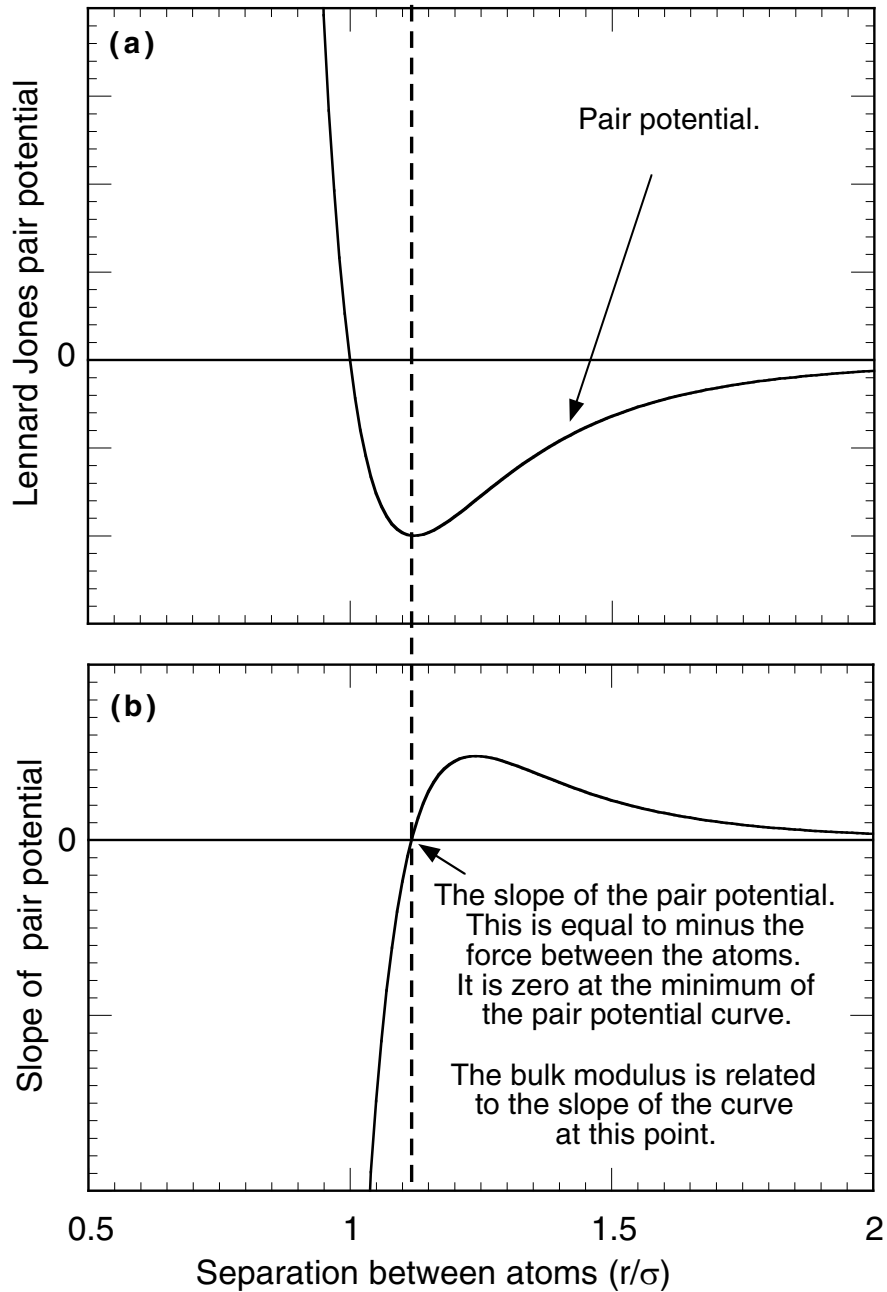
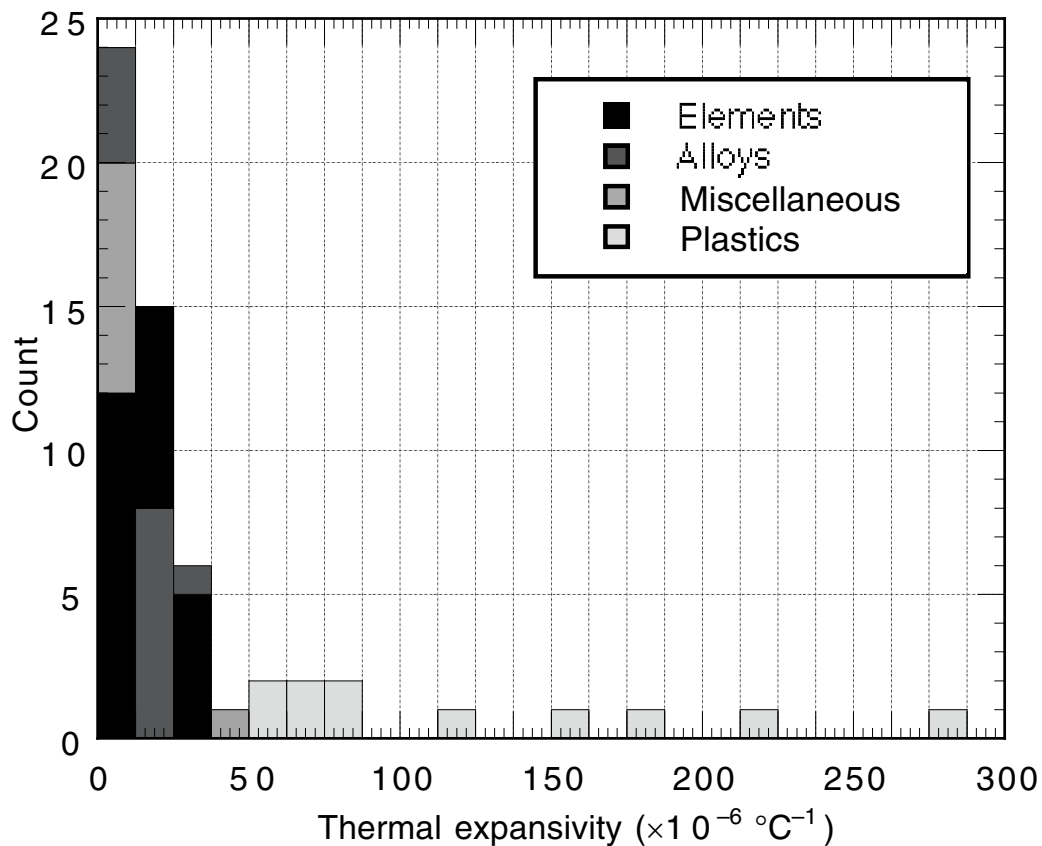


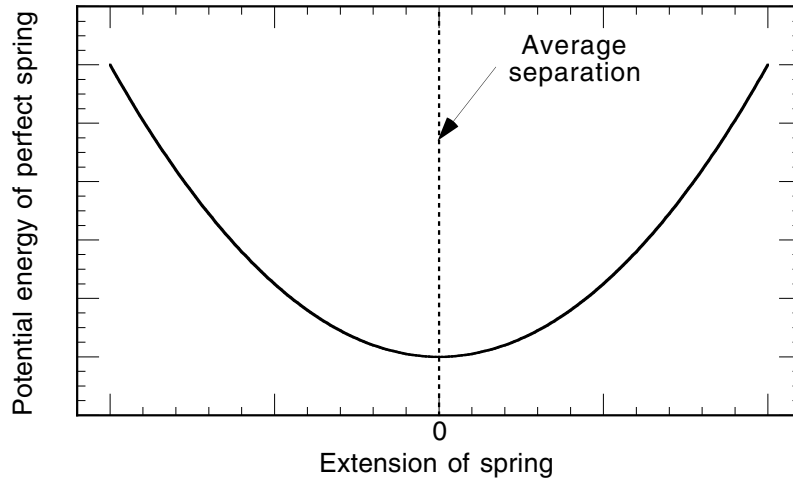
Figure 7.6 Histogram of the data from Table 7.4 Where a range of values indicated in Table 7.4 the mid-point of the range has been used for plotting purposes.



Extracted from *Understanding the properties of matter* by Michael de Podesta.
The copyright of these figures resides with *Taylor and Francis*.
They may be used freely for educational purposes but their source must be acknowledged.
For more details see www.physicsofmatter.com

Figure 7.7 The potential energy of interaction between atoms in a solid. (a) The *harmonic approximation*: How the energy would vary if the atoms were connected by ‘perfect springs’. (b) The typical deviation from the harmonic approximation of a real interatomic potential. The sloping line indicates the increasing average separation as the average energy of oscillation (i.e. the temperature) is increased.

(a)



(b)

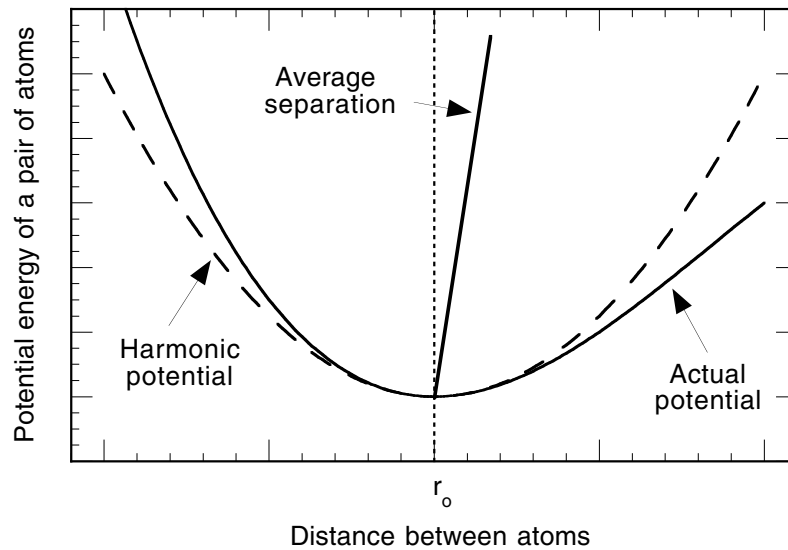
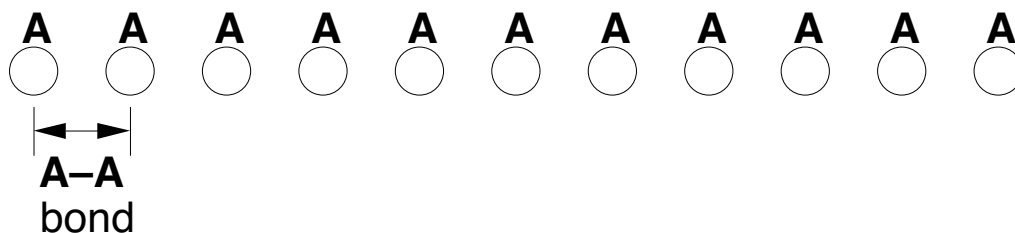
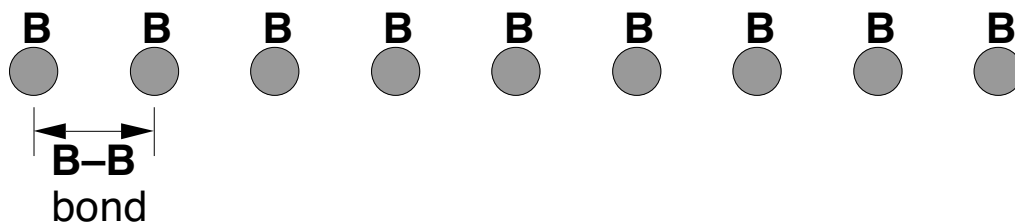


Figure 7.8 An illustration of the arrangement of bonds in one-dimensional models of pure A, pure B, and an alloy of A and B. Notice that the alloy contains an type of interatomic bond which is present in neither of the pure substances.

Pure A



Pure B



AB alloy

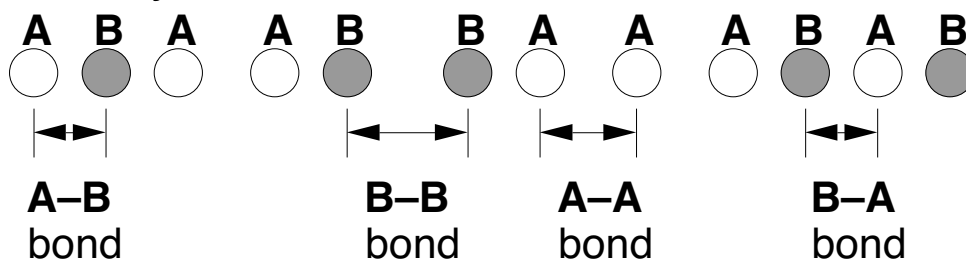
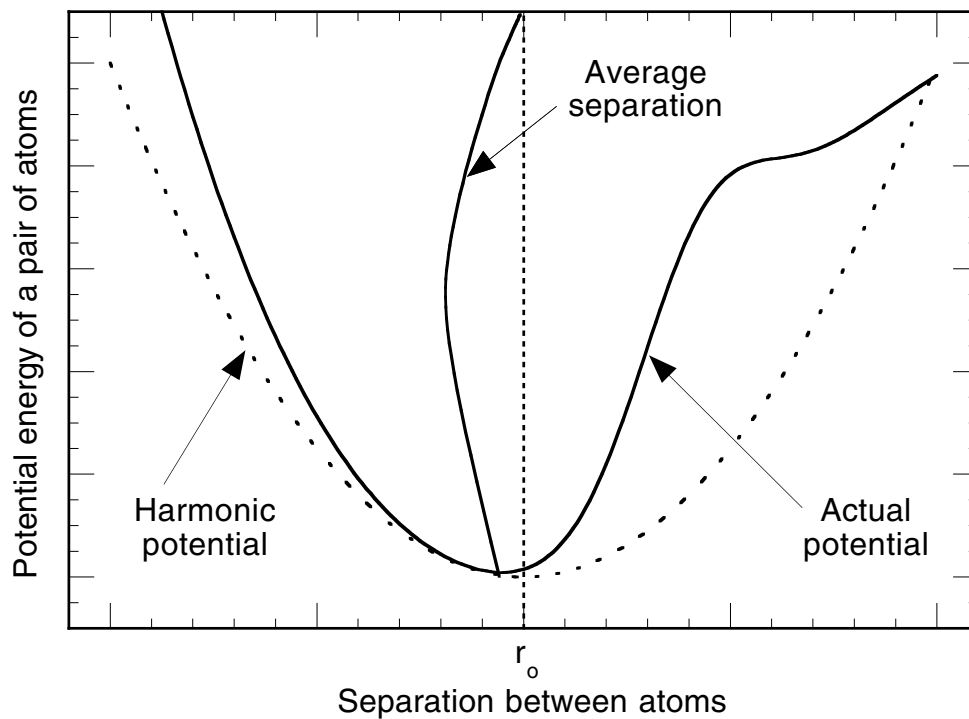


Figure 7.9 Schematic illustration of the potential energy of an Fe–Ni bond in an invar alloy (Table 7.8). The asymmetry of the potential (over a certain range) is opposite to that which occurs in normal bonds (Figure 7.7).



Extracted from *Understanding the properties of matter* by Michael de Podesta.
The copyright of these figures resides with Taylor and Francis.
They may be used freely for educational purposes but their source must be acknowledged.
For more details see www.physicsofmatter.com

Figure 7.10 The variation of the speed of longitudinal and transverse sound waves (Table 7.9) with relative atomic mass. For comparison, a section of the data for gases from Table 5.14 is also plotted. There appears to be a tendency towards lower speeds at larger atomic masses, similar to the tendency shown by gases in Figure 5.19. Data points are joined by straight lines to highlight trends in each data set.

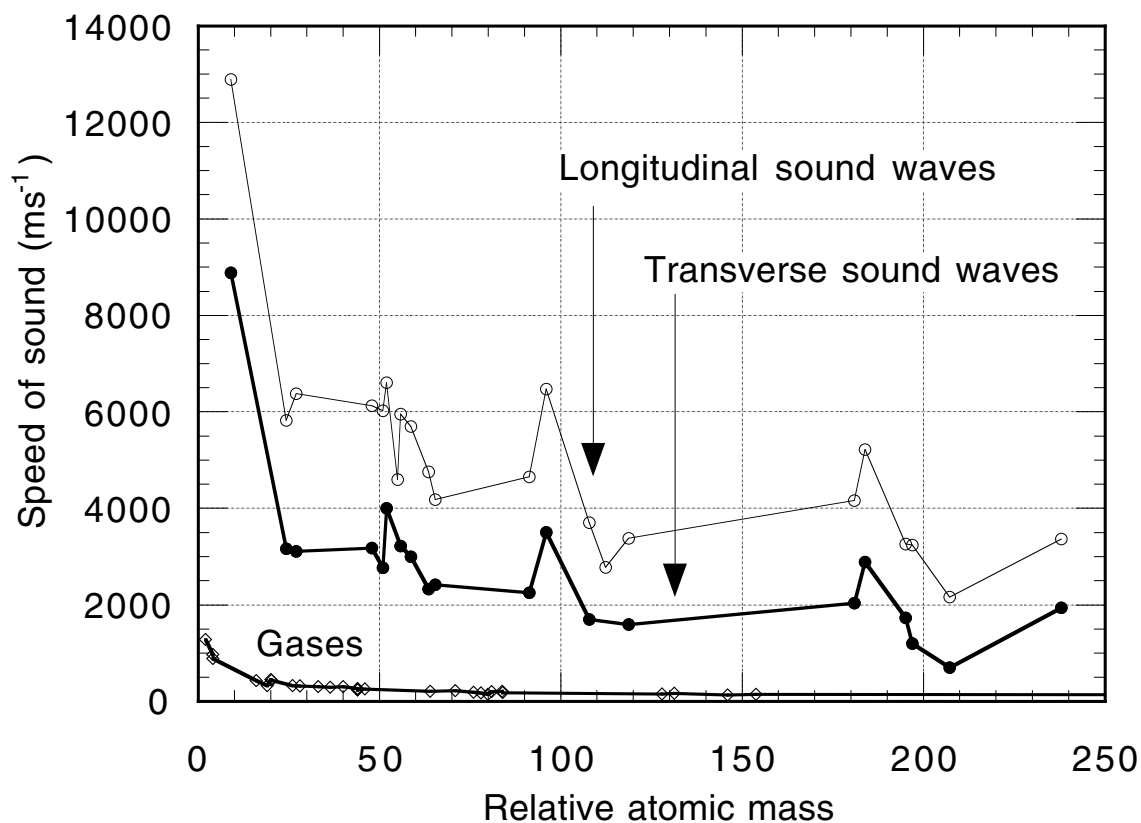
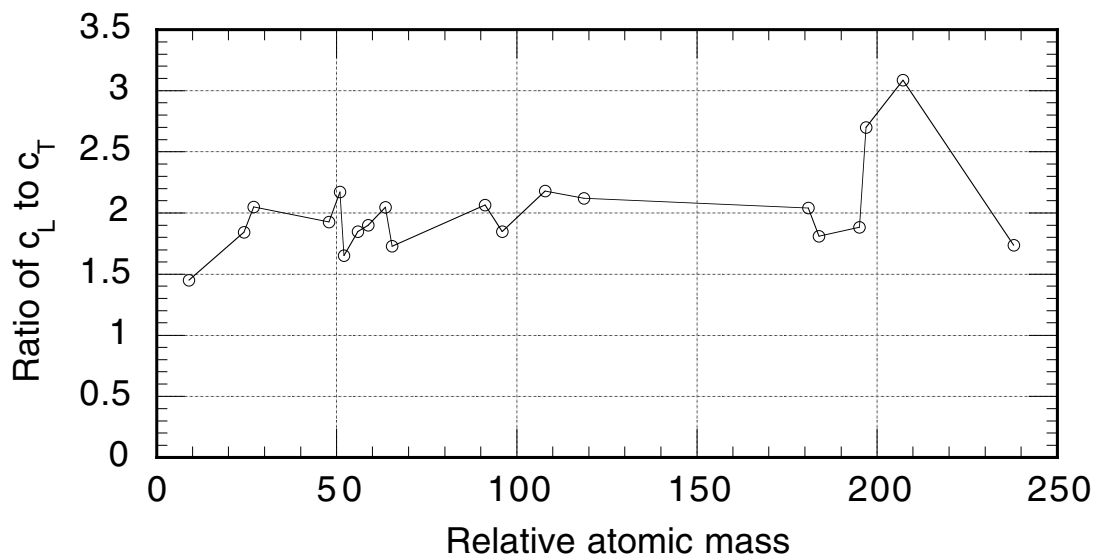


Figure 7.11 The variation of the ratio of the longitudinal to transverse sound velocities with relative atomic mass for the elements in Table 7.9. Typically $c_L \approx 2c_T$, but in some cases the results differ significantly from this value.



Extracted from *Understanding the properties of matter* by Michael de Podesta.
The copyright of these figures resides with Taylor and Francis.
They may be used freely for educational purposes but their source must be acknowledged.
For more details see www.physicsofmatter.com

Figure 7.12 Sound waves in solids: (a) longitudinal (b) and (c) transverse waves. The figure shows planes of material perpendicular to the direction of propagation of a sound wave. In the longitudinal wave (a) the strength of shading indicates the degree of compression or rarefaction. In (b) and (c) a transverse wave displaces layers of material perpendicular to the direction of propagation. In (b) the layers are displaced from side to side and in (c) they are displaced up and down.

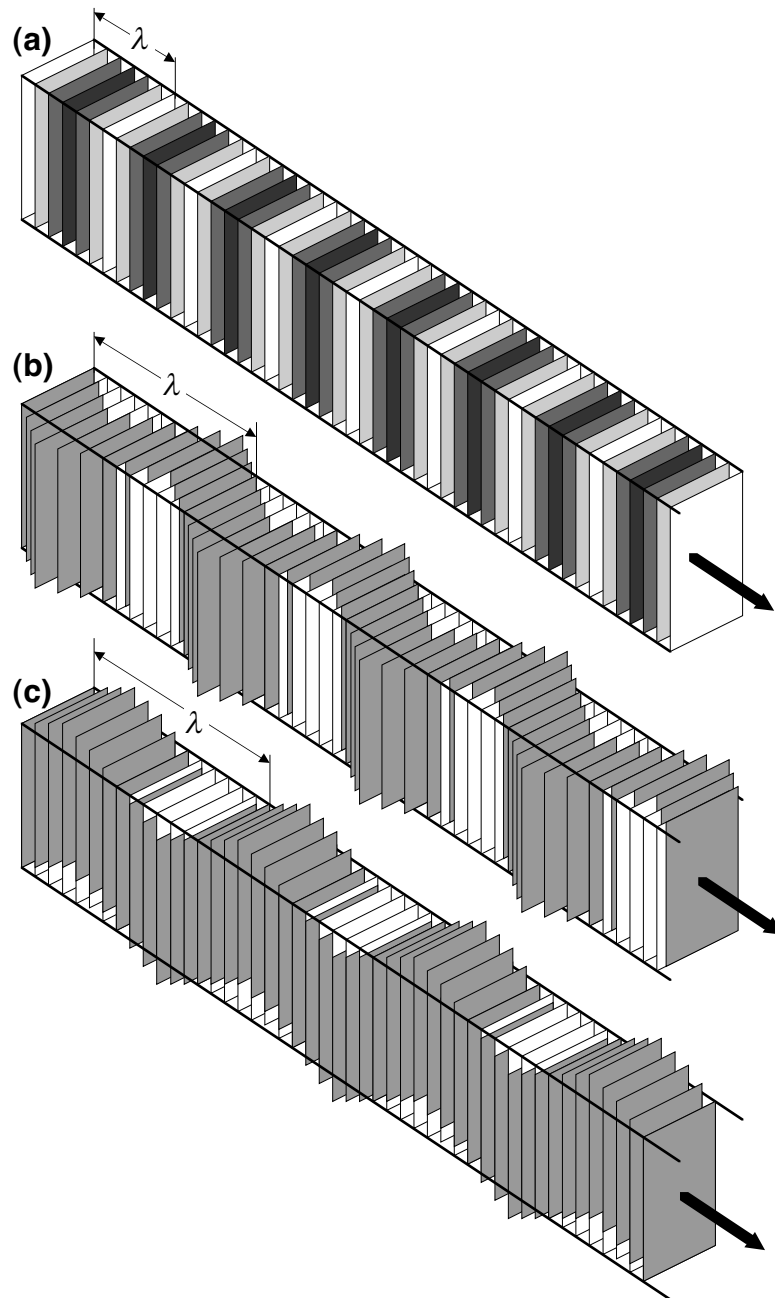


Figure 7.13

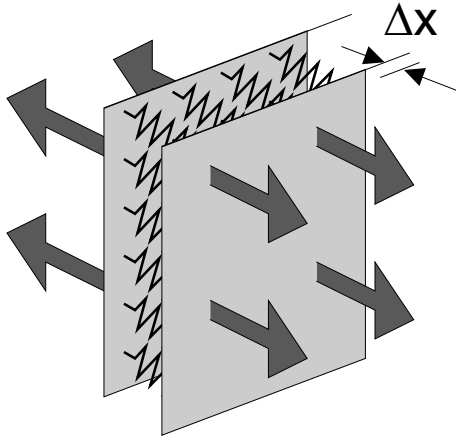


Figure 7.16

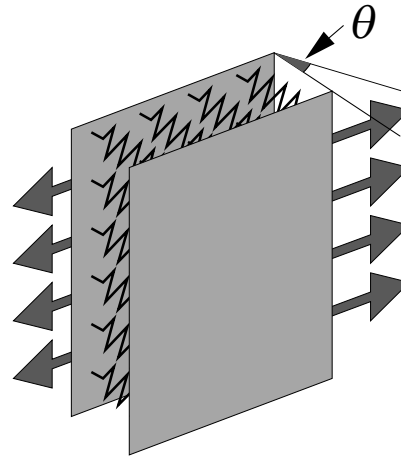


Figure 7.14 (a) Two planes in a solid in their equilibrium position. In (b) and (c) the same planes are subject to two types of shear strain and in (d) to compressive strain.

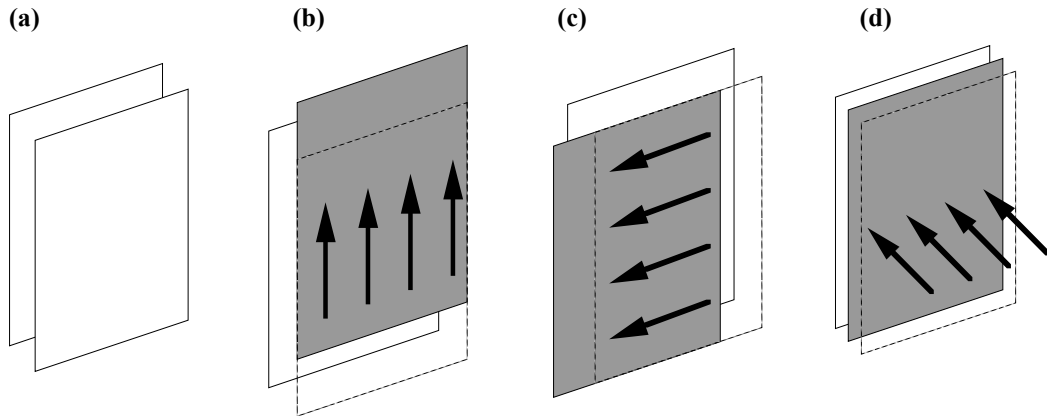
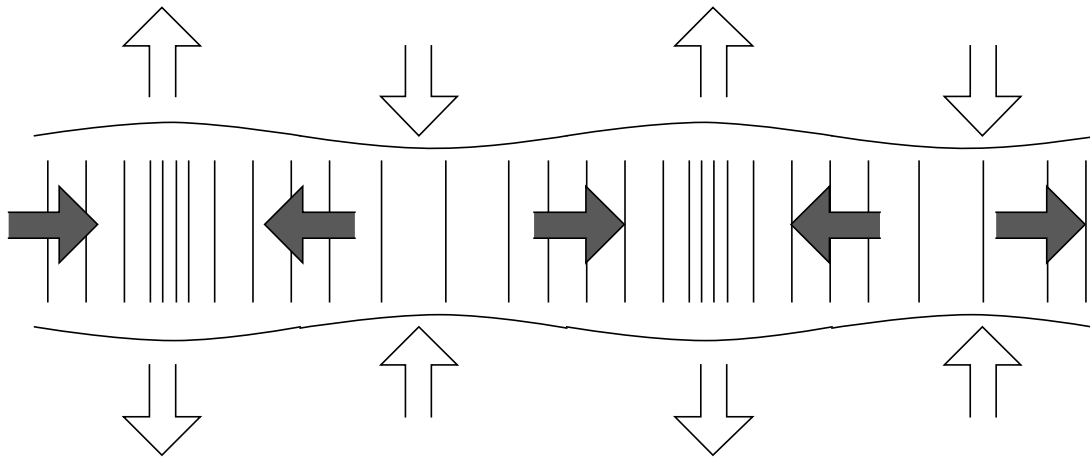
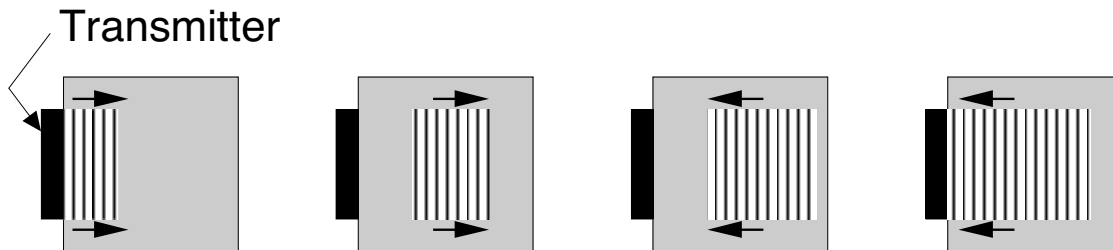


Figure 7.15 Illustration of the way in which a rod of material necks and bulges as a compressive sound wave travels along a long thin rod.



From Example 7.7



From Example 7.8

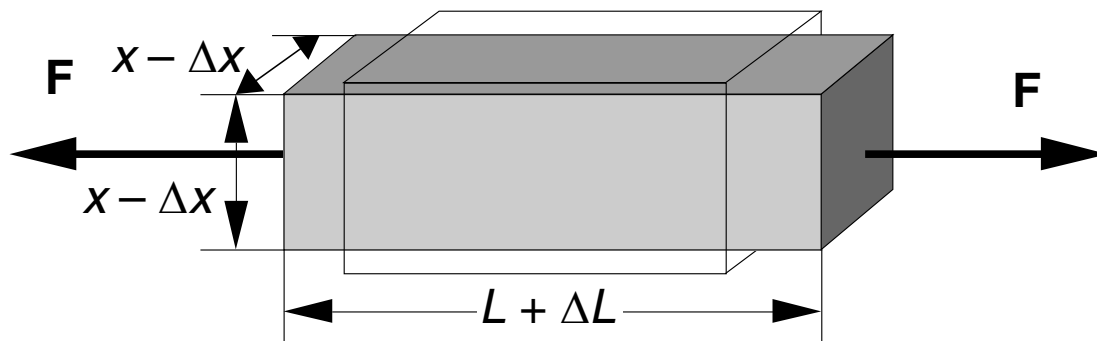
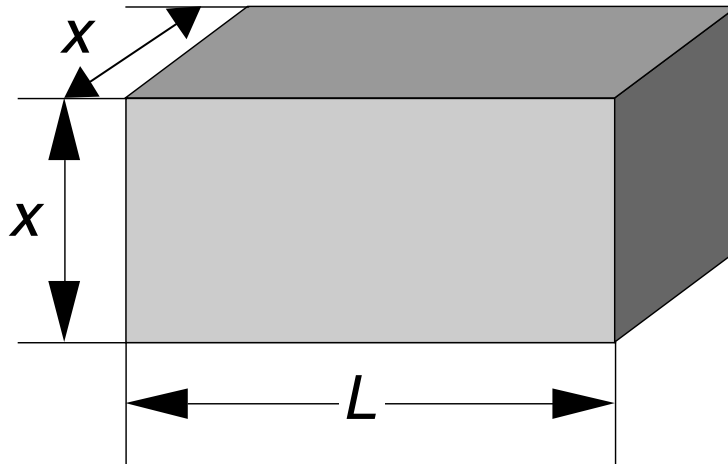


Figure 7.17 A simple prediction for the speed of longitudinal sound waves in the elements assuming that:

- All elements have the same value of Young's modulus E of ≈ 100 GPa
- All elements have Poisson ratio $\approx 1/3$
- The density of the elements is given by the formula (Example 7.2) $\rho = 61.5A$.

The final formula evaluated is $c_L = \sqrt{1.5 \times 10^{11} / 61.5A}$

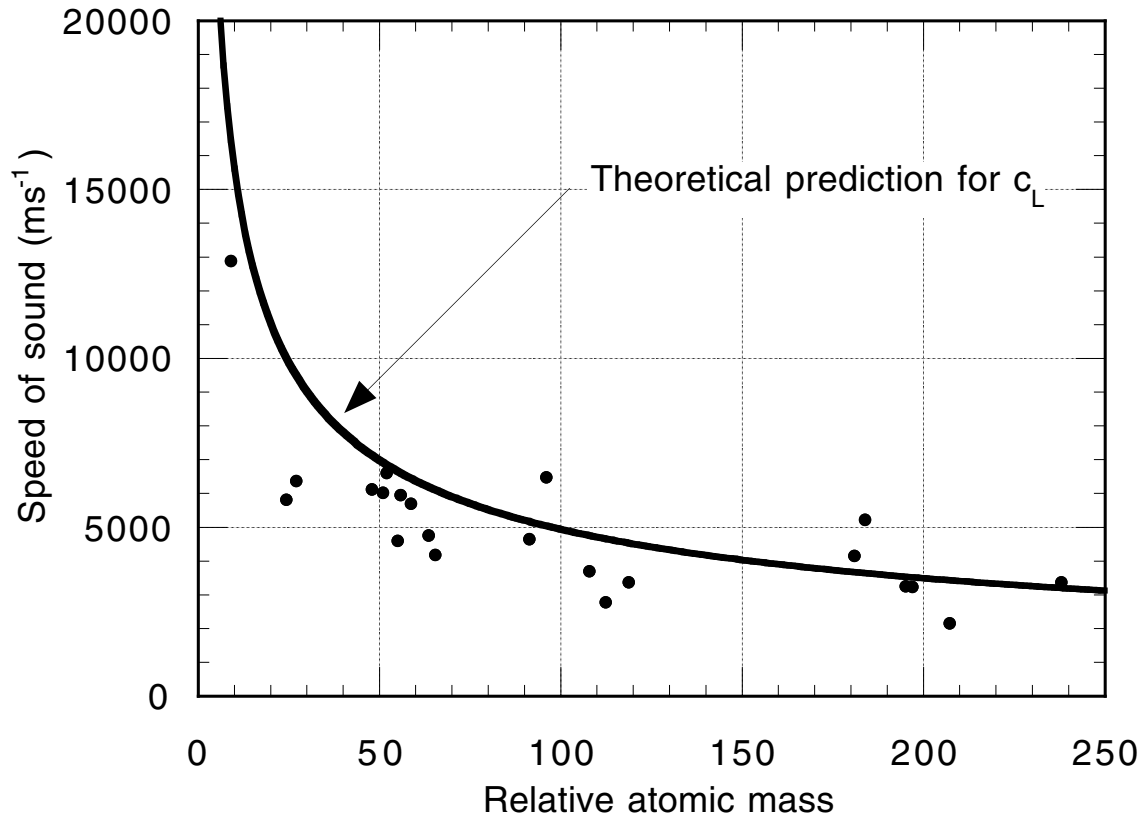


Figure 7.18 Histogram of C_p for the solid elements in $\text{J K}^{-1} \text{mol}^{-1}$ at around room temperature ($25^\circ\text{C} = 298.15 \text{ K}$). More than 50% of the elements have a heat capacity close to $25 \text{ J K}^{-1} \text{mol}^{-1}$, and nearly all elements have C_p between 22 and $32 \text{ J K}^{-1} \text{mol}^{-1}$.

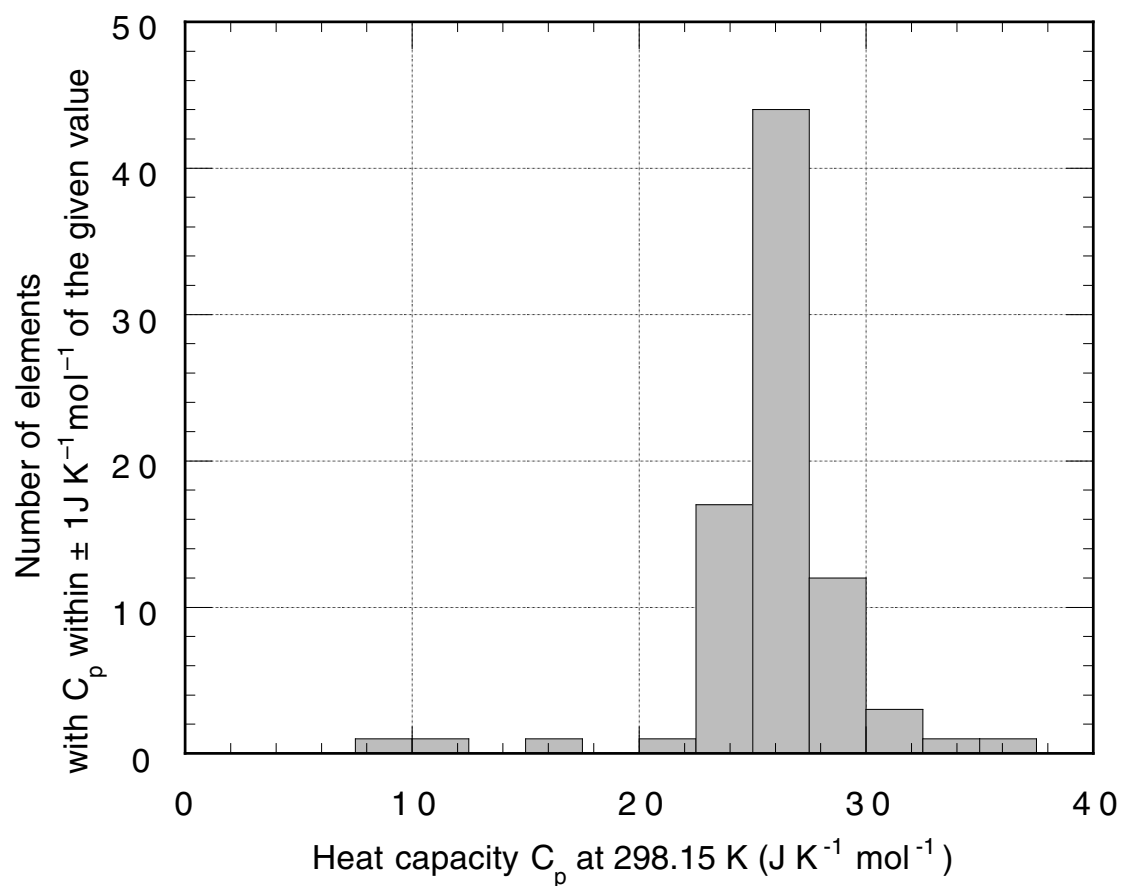


Figure 7.19 The variation with temperature of the molar heat capacity of copper, silver and gold. All three curves tend to a value $\approx 25 \text{ J K}^{-1} \text{ mol}^{-1}$ at high temperatures in accord with the results of Table 7.10 and Figure 7.18. At low temperatures all three curves tend to zero.

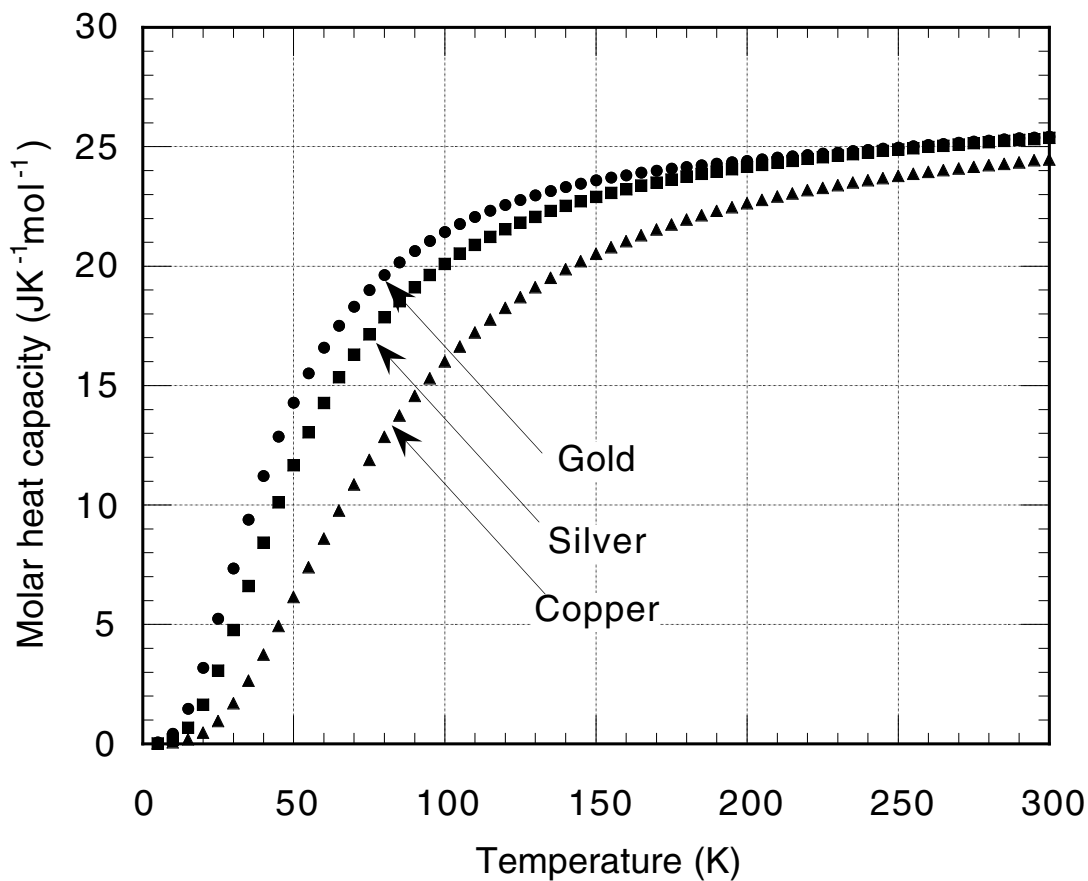


Figure 7.20 The variation with temperature of the heat capacity of sapphire (Al_2O_3). The data tends to a value $\approx 130 \text{ J K}^{-1} \text{ mol}^{-1}$ at high temperatures, much higher than the elemental values of Table 7.10 and Figure 7.18. At low temperatures the data tend to zero in a similar manner to the data for copper, silver and gold (Figure 7.19)

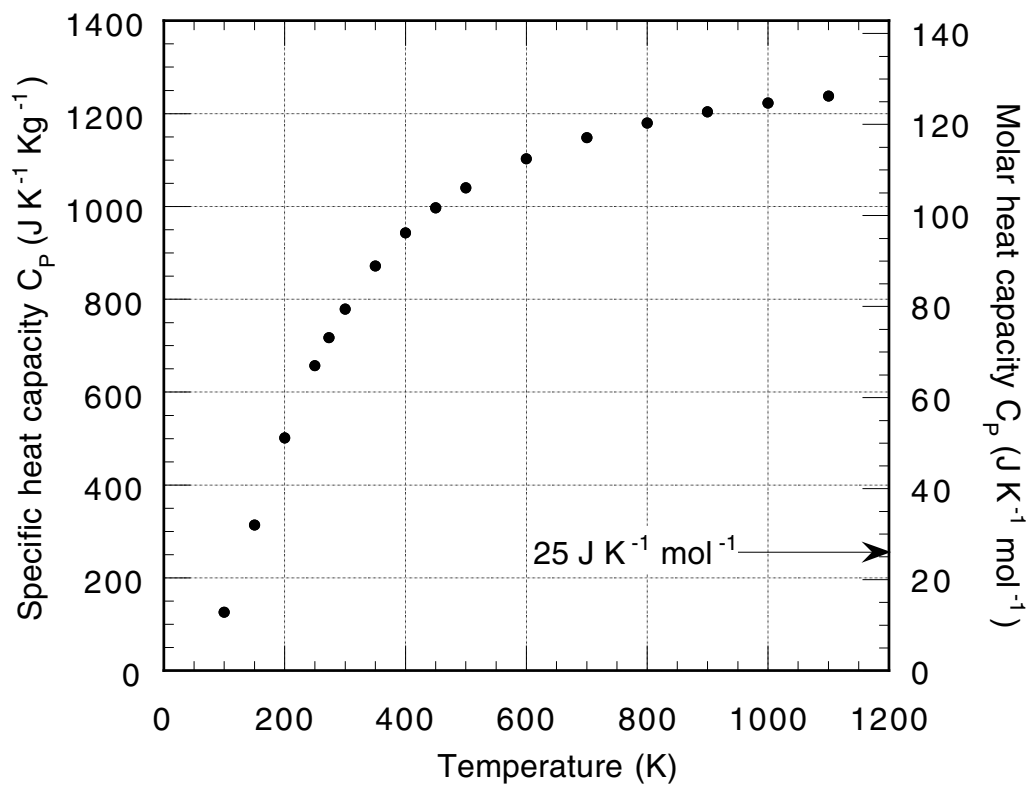


Figure 7.21 Analogy to the situation of atoms in a crystal. An atom behaves *as if* it were held at its minimum energy position by springs. First (a) shows the atom in its equilibrium position and (b) shows the atom displaced from its equilibrium position. Notice that the springs in (b) are all either compressed or extended compared with their equilibrium length of r_0 .

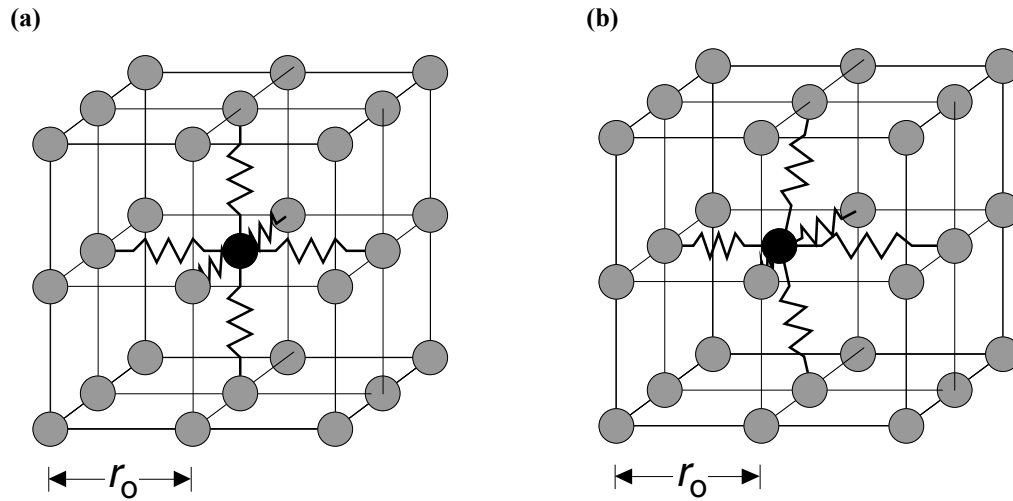


Figure 7.22 An illustration of two simple harmonic potentials with different spring constants. A given amount of energy (for example $0.5 k_B T$) results in smaller oscillations of the stiffer-springed potential.

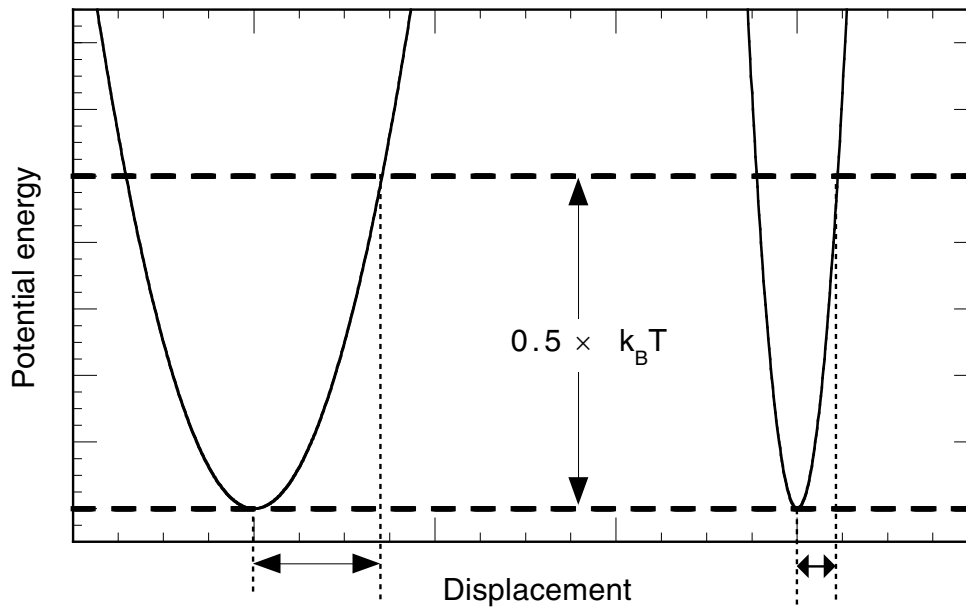


Figure 7.23 Histogram of the heat capacities at constant pressure C_p of the solid elements in $\text{J K}^{-1} \text{mol}^{-1}$ at room temperature $25\text{ }^\circ\text{C} = 298.15\text{ K}$ (also shown as Figure 7.18). The bold line shows the prediction of Equation (7.42) for the heat capacity of all elements.

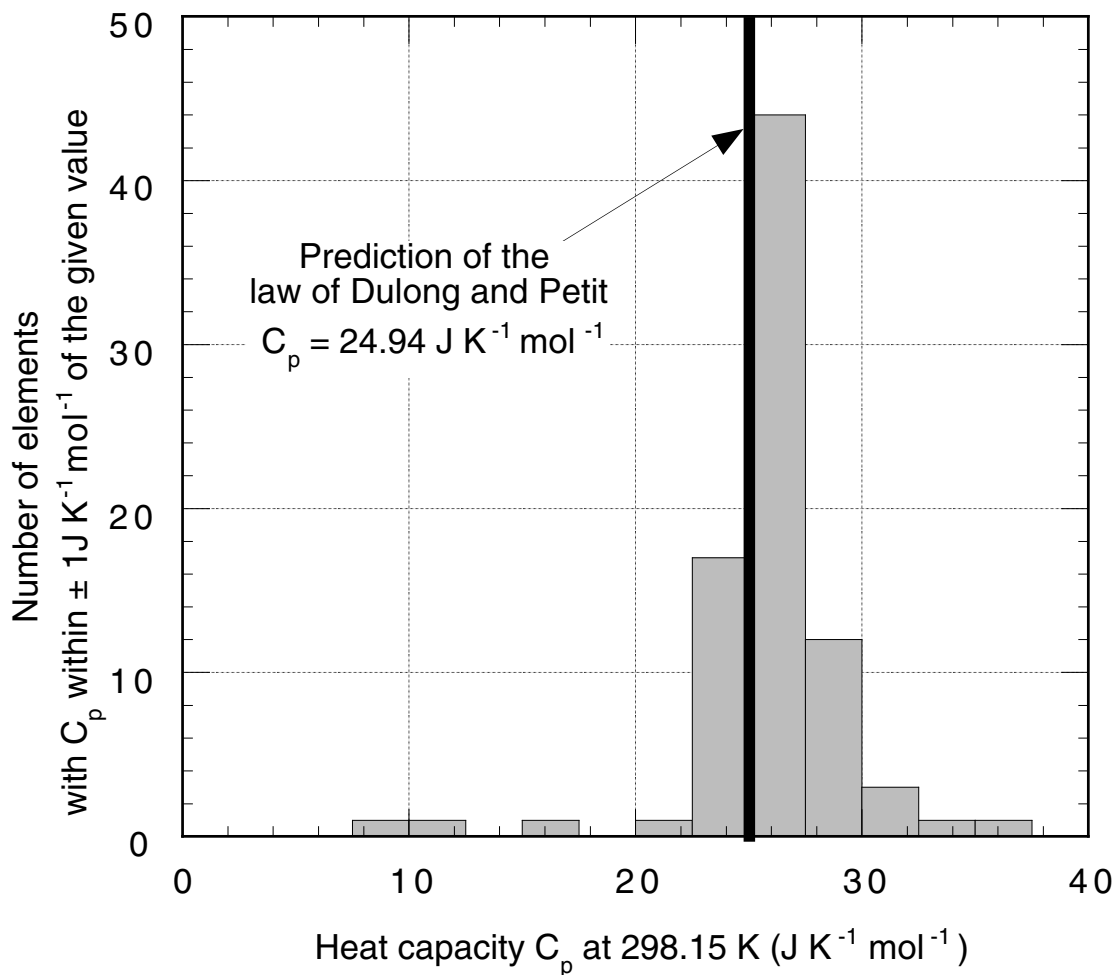


Figure 7.24 An illustration of the relationship between energy levels, particle mass and spring constant for a simple harmonic potential. If (a) represents the energy levels of a particle of mass M bonded in a particular way, then (b) would represent the energy levels of a heavier particle in the same potential, and (c) would represent the energy levels of a particle of a similar mass, but more stiffly constrained.

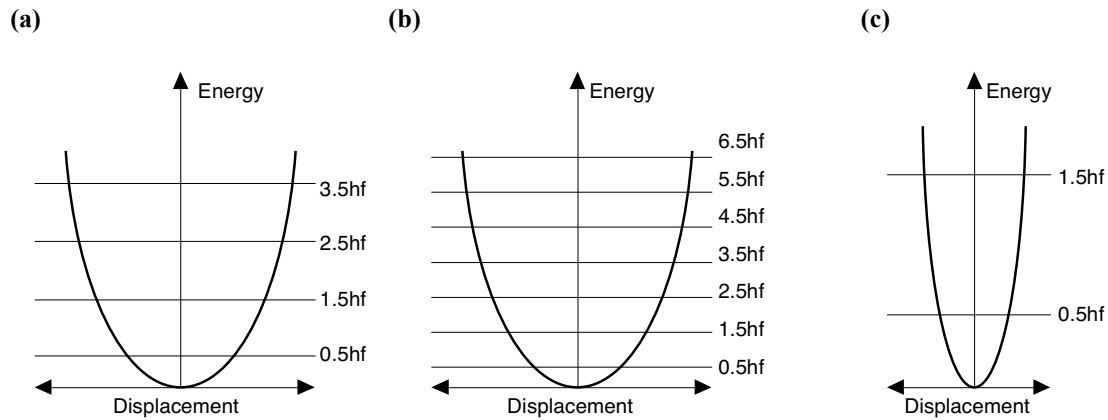


Figure 7.25 The heat capacity of copper from Figure 7.19 plotted together with the Einstein prediction for the heat capacity based on $\Theta_E = 230$ K. The predicted Einstein temperature corresponds to a spring constant of $K = 2.423$ J m⁻², and a frequency of vibration of $f_0 = 4.79 \times 10^{12}$ Hz. It is clear that the theory captures the trend of the data. However, careful examination shows that the agreement between the theory and experiment becomes poor at low temperatures. **Note:** The Einstein theory prediction is for C_V , but the data with which it is compared is based on C_p .

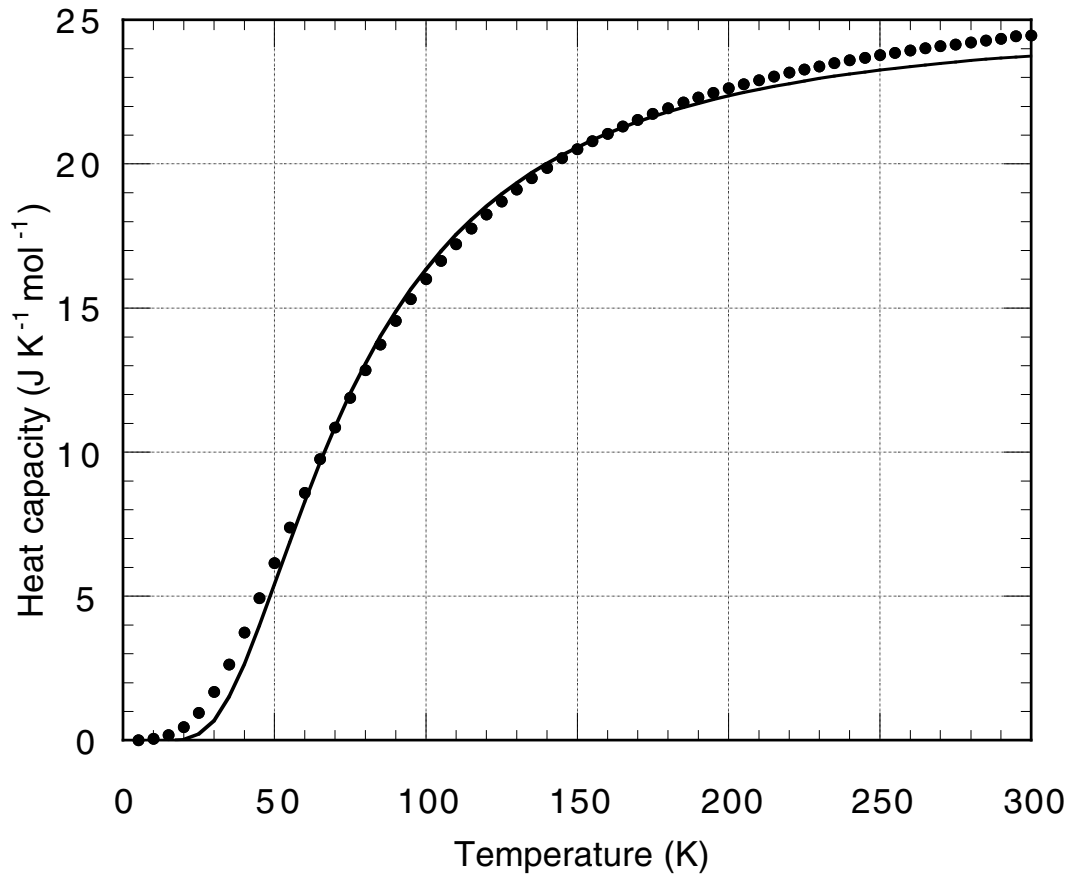
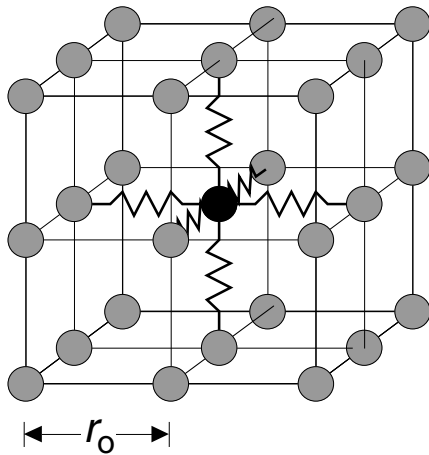


Figure 7.26 Analogy to the situation of atoms in a crystal. The forces on an atom are such that the atom behaves *as if* it were held at its minimum energy position by springs. First (a) shows the simple model used in our initial analysis, then (b) shows a more realistic representation of the situation within the solid. Motion of the central atom in (b) causes all the atoms around it to move as well, creating a tremendously difficult situation to analyse.

(a)



(b)

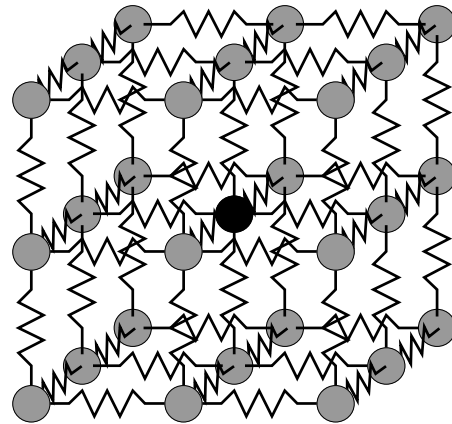
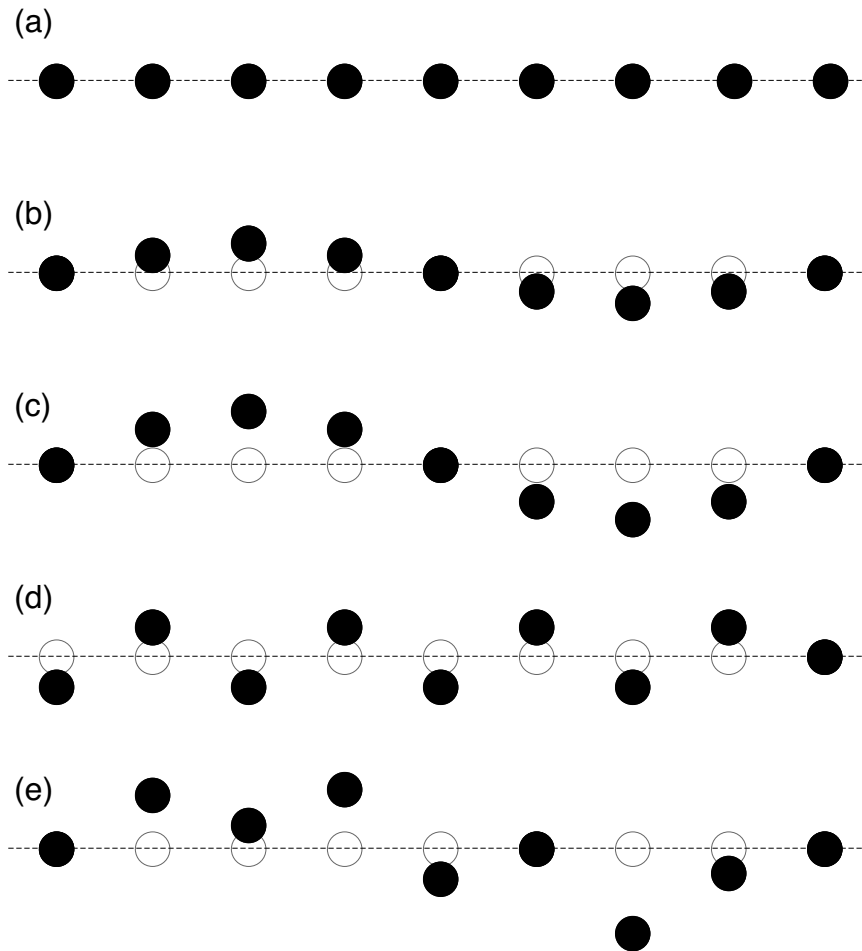


Figure 7.27 Illustration of the concept of a phonon in 1-dimensional crystal. The filled circles represent the instantaneous positions of atoms and the empty circles represent their equilibrium positions. Case (a) shows the crystal when there are no phonons present. Case (b) would be described by saying there is one transverse phonon present in the lattice with relatively long wavelength λ_1 and relatively low frequency f_1 . In case (c) the amplitude of the wave is larger than in (b) which would be described by saying there are two transverse phonons with the same wavelength λ_1 and relatively low frequency f_1 as in (b). Case (d) would be described by saying there is one transverse phonon present in the lattice with relatively short wavelength λ_2 and relatively high frequency f_2 . Case (e) would be described by saying there are two transverse phonons in the lattice: one with long wavelength and low frequency and other with short wavelength and high frequency.



Extracted from *Understanding the properties of matter* by Michael de Podesta.
The copyright of these figures resides with *Taylor and Francis*.
They may be used freely for educational purposes but their source must be acknowledged.
For more details see www.physicsofmatter.com

Figure 7.28 The relationship between frequency and wavelength assuming a speed of sound of 4000 ms^{-1} . For wavelengths less than an atomic spacing (typically $3 \times 10^{-10} \text{ m}$), the idea of a compression wave becomes meaningless, because there is nothing to be compressed! This estimates that the maximum frequency of atomic vibrations is $\approx 10^{13} \text{ Hz}$.

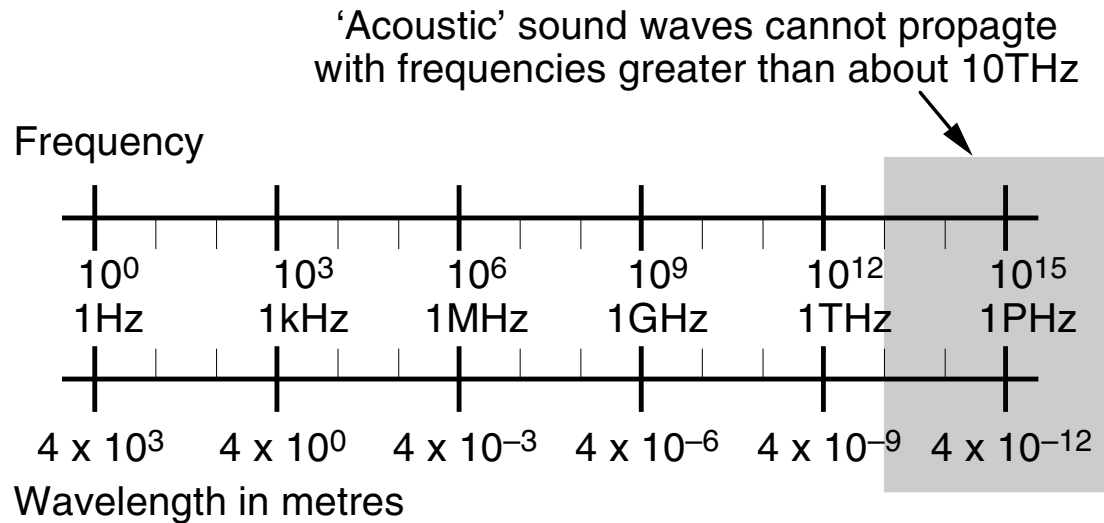


Figure 7.29 The Debye prediction for the heat capacity of copper compared with the Einstein prediction shown in Figure 7.25.

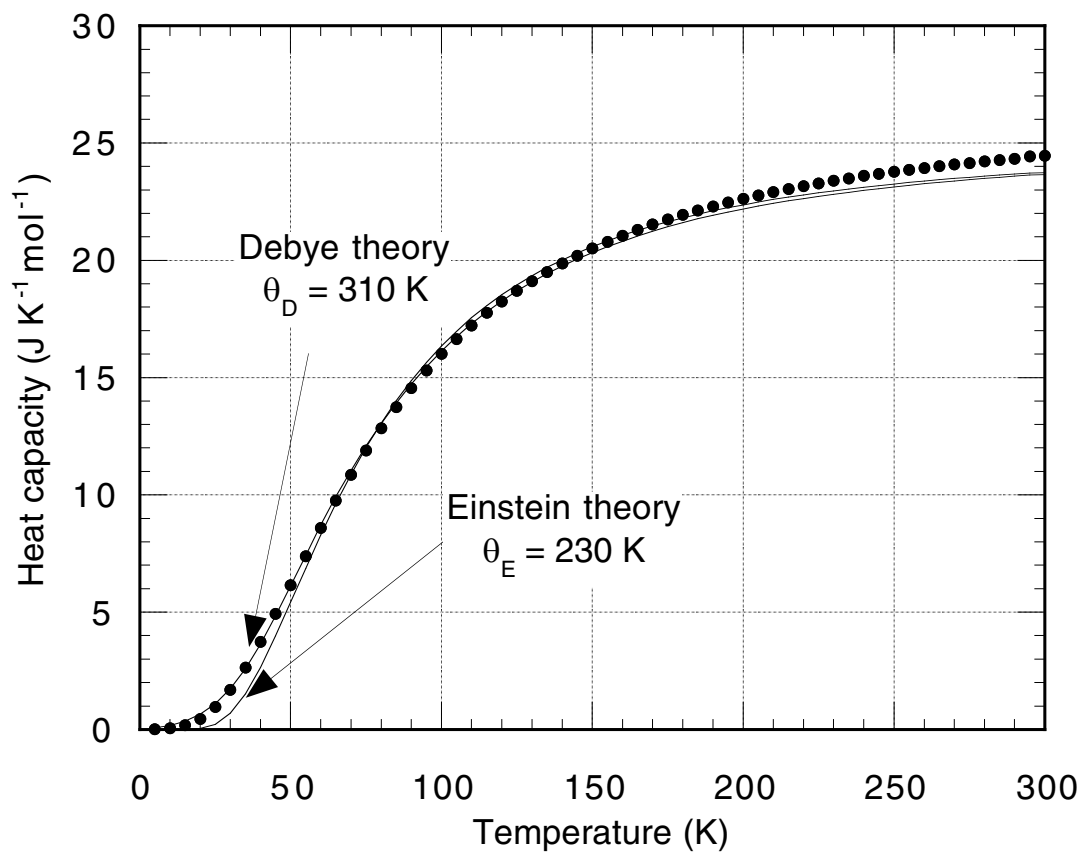


Figure 7.30 The Debye prediction for the heat capacity of solids with Debye temperatures of 100 K, 300 K and 1000 K. At room temperature, the heat capacity values will be close to $C_V = 3R$ if Θ_D is less than room temperature. However if Θ_D is much greater than room temperature, then the heat capacity at room temperature appears to anomalously low. This is the origin of the anomalously low values of C_p for beryllium, boron and carbon in Figure 7.18.

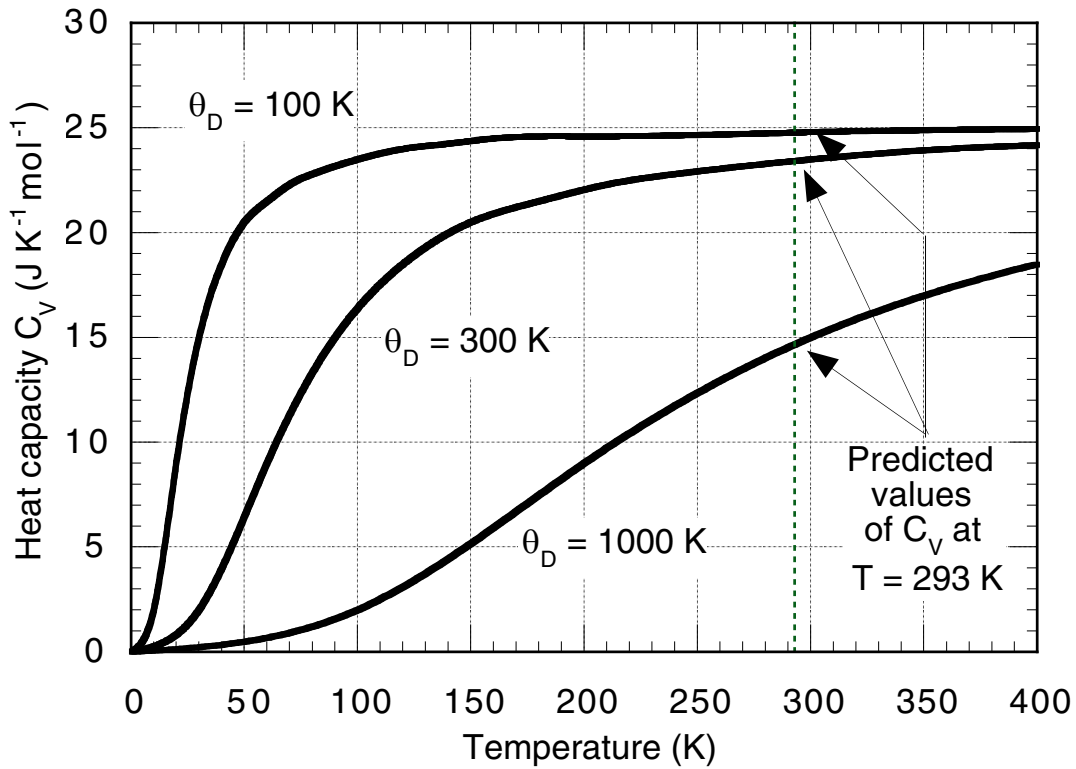


Figure 7.31 The speed of transverse sound waves in some elements (Table 7.9) plotted as a function of their Debye temperature (Table 7.12). It is clear that there is a roughly linear relationship between the two quantities.

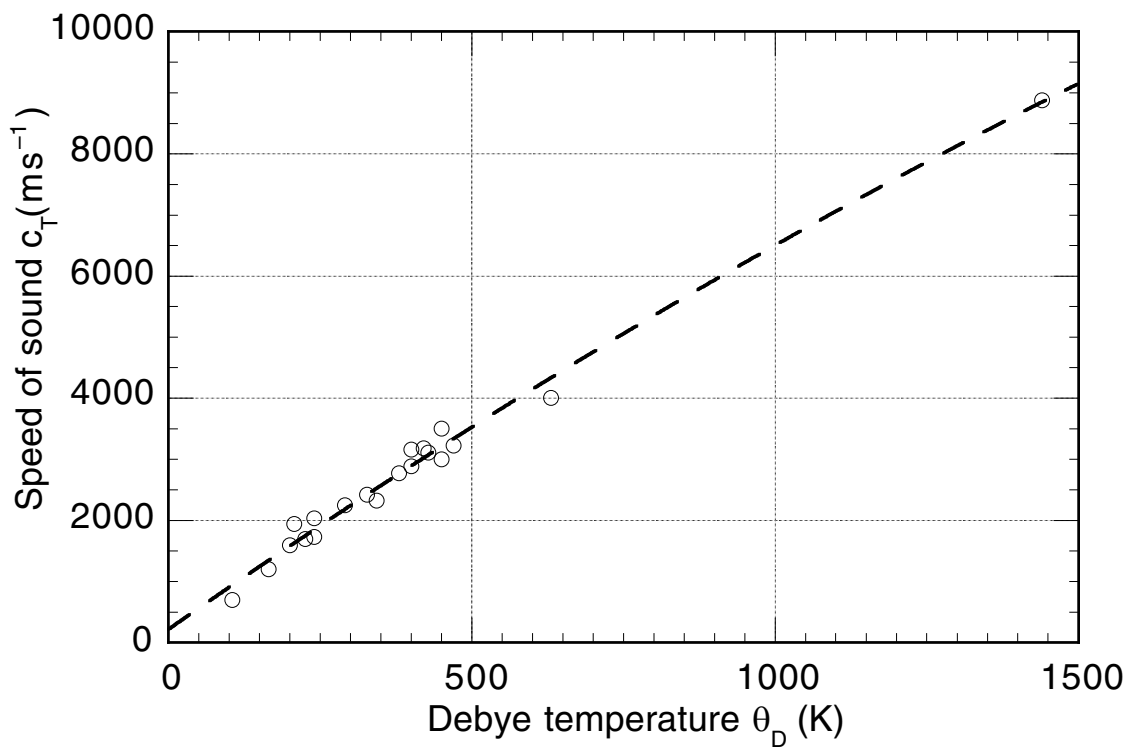


Figure 7.32. A close-up view of the occupation of quantum states in the region near the occupied quantum states with the maximum energy of E_F . A filled circle represents an occupied quantum state, and an empty circle represents an empty quantum state. As the temperature increases, electrons in quantum states within a range $\approx \pm k_B T$ of E_F can change states. The exclusion principle prevents electrons in states with energy much more than $\approx k_B T$ below the maximum energy from accepting energy. This is because there are no vacant states for these electrons to move into.

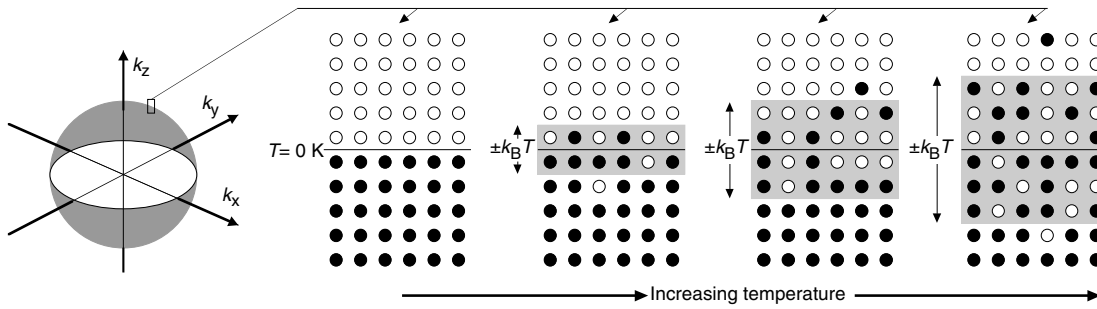


Figure 7.33 My own measurements of the low-temperature heat capacity of copper plotted as C/T versus T^2 . Since the graph has T squared as its x -axis, the data shown correspond to the temperatures between 2 K and 10 K. Note that as predicted by Equation 7.71, the data conform to a straight line. From the slope of the line, α and hence the Debye temperature can be found, and from the intercept we may determine γ and hence $g(E_F)$.

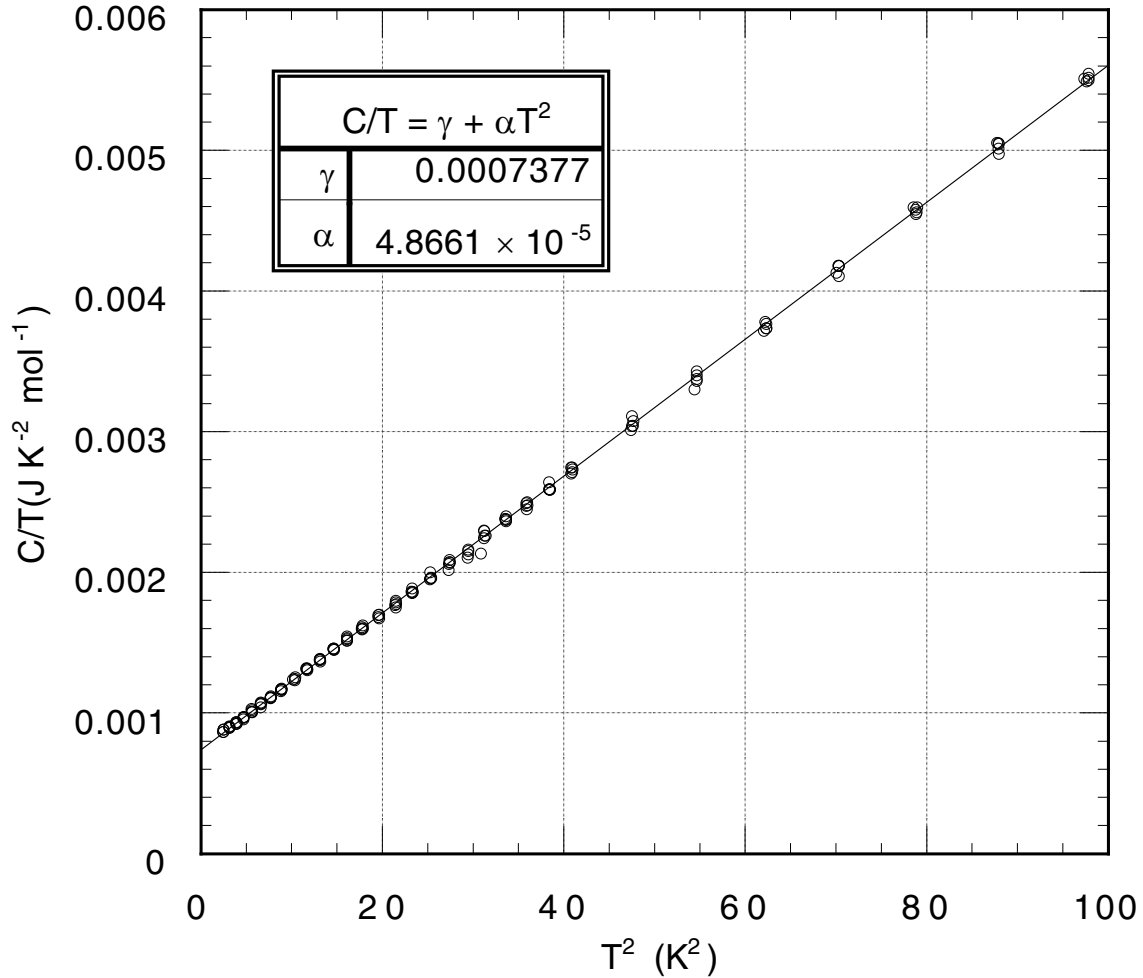


Figure 7.34 The logarithm of the resistivity of the elemental metals (M), semiconductors (SC) and insulators (Ins) plotted as a function of atomic number. The elemental gases are plotted as having a resistivity of $10^{20} \Omega\text{m}$ to show how they fit the pattern of conducting and insulating behaviour.

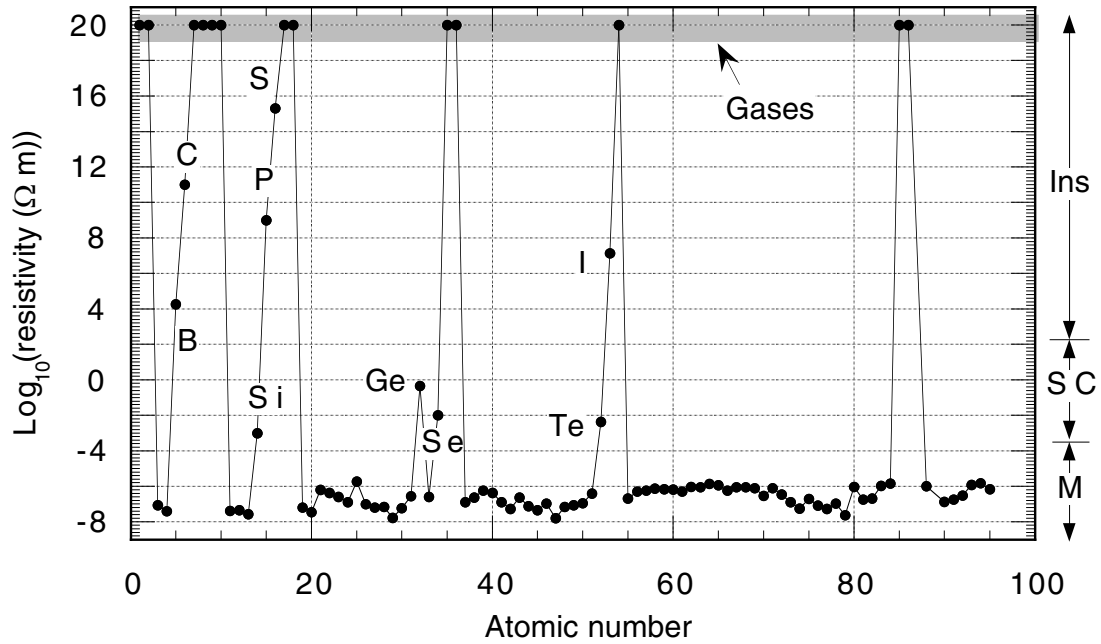


Figure 7.35 The resistivities of the metallic elements plotted on a linear scale as a function of atomic number. Elements with date off the graph have not been plotted.

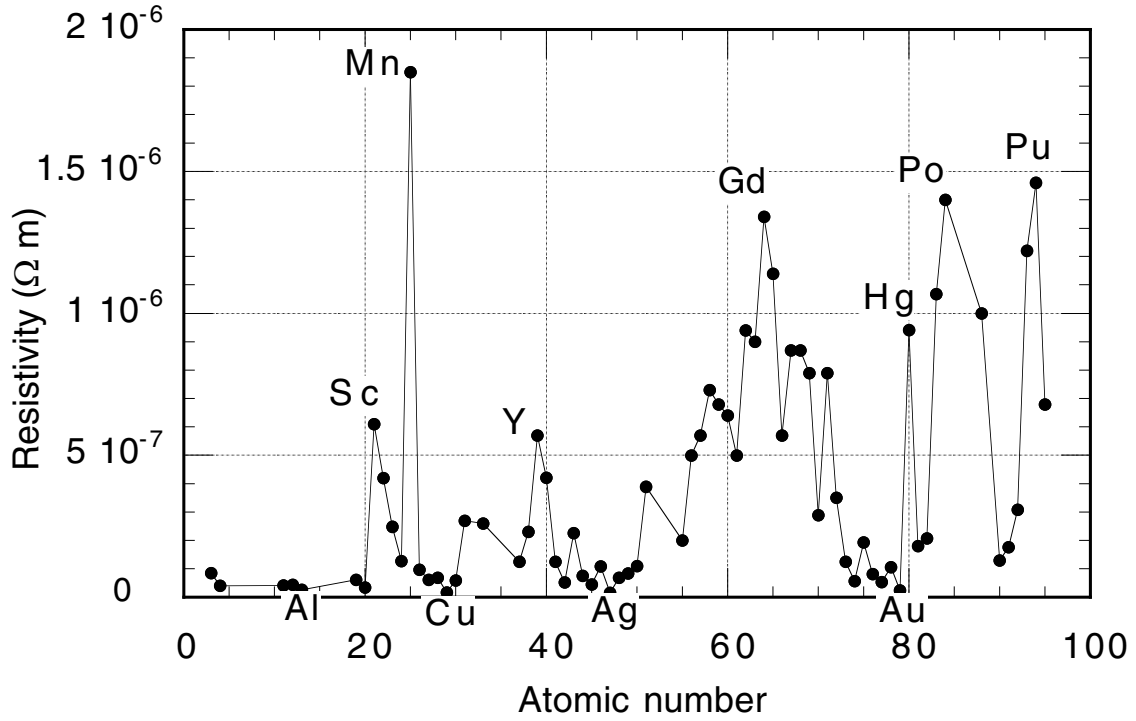


Figure 7.36 The resistivities of five metallic elements plotted on a linear scale as a function of temperature. The data for platinum is the result of many closely-spaced measurements and is plotted as a continuous curve. The data for Al, Cu, Ag and Au consists of just a few points with lines drawn to connect the data points.

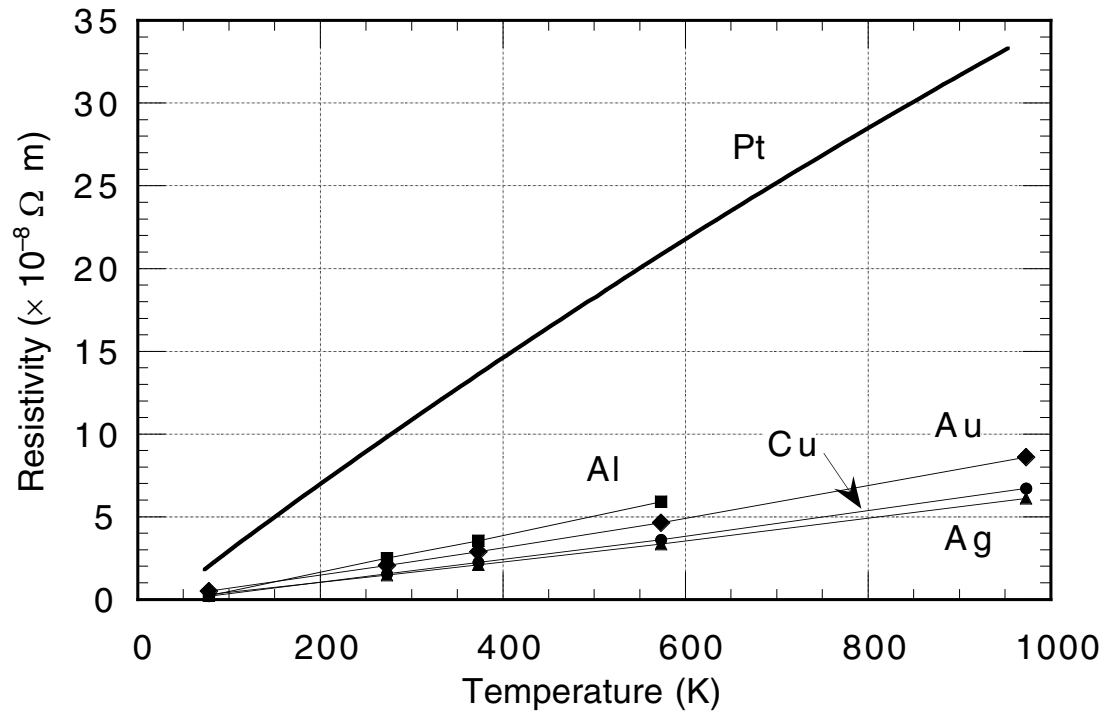
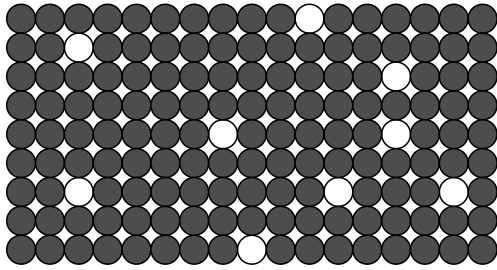


Figure 7.37 illustration of the difference between (a) a random binary alloy, and (b) a mixture of two elements.

(a)



(b)

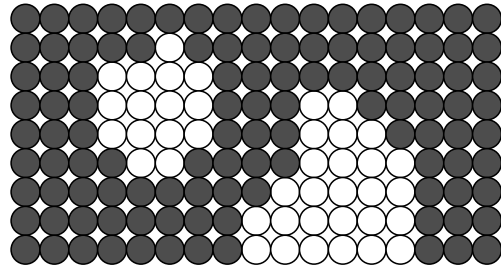


Figure 7.38 Illustration of the effect of an electric field on the occupation of quantum states in a simple model of a metal. First, (a) shows the case when no electric field is applied, then (b) shows the case when an electric field is applied in the negative- x direction. Notice that in (b) the distribution is not symmetric but is shifted by an amount Δk and so has a net excess of electrons with positive k -vectors. In the figures each small circle represents an allowed travelling wave solution to the Schrödinger equation. The shaded circle represents the Fermi sphere of occupied states which is shifted by Δk as discussed in the text.

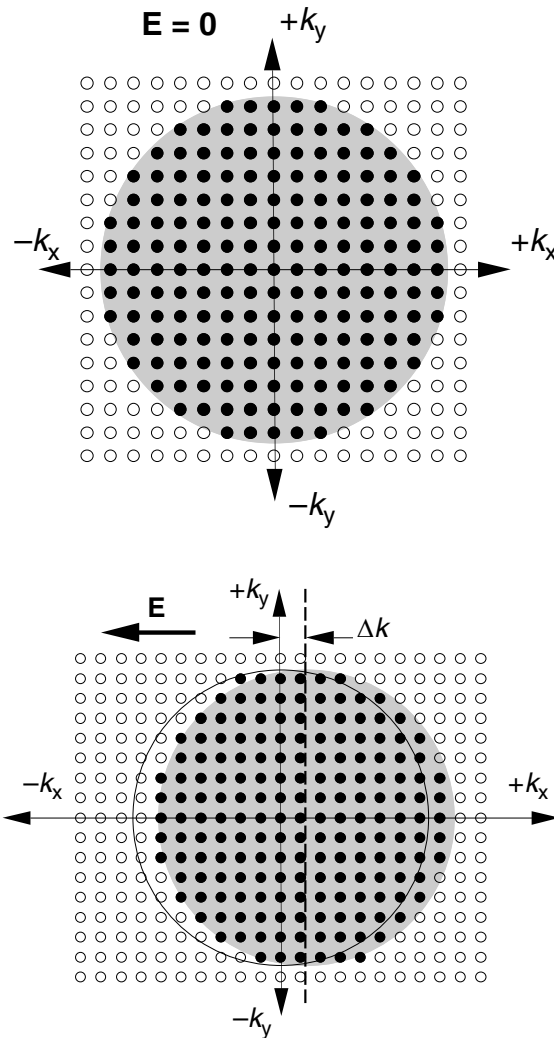
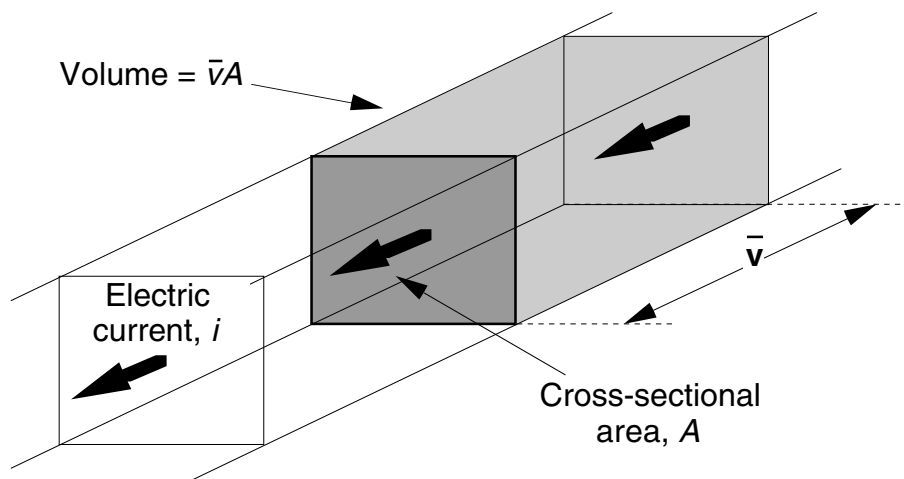


Figure 7.39 Electrons flowing through a piece of metal. In one second all the charge within a distance \bar{v} 'upstream' of a cross-section perpendicular to the current flow will pass the cross-section. In this case the volume of charge that will flow past the cross sectional area is $\bar{v}A$. The amount of charge in this volume is $qnA\bar{v}$



Extracted from *Understanding the properties of matter* by Michael de Podesta.
The copyright of these figures resides with *Taylor and Francis*.
They may be used freely for educational purposes but their source must be acknowledged.
For more details see www.physicsofmatter.com

Figure 7.40: Arrangements of atoms in a binary alloy.

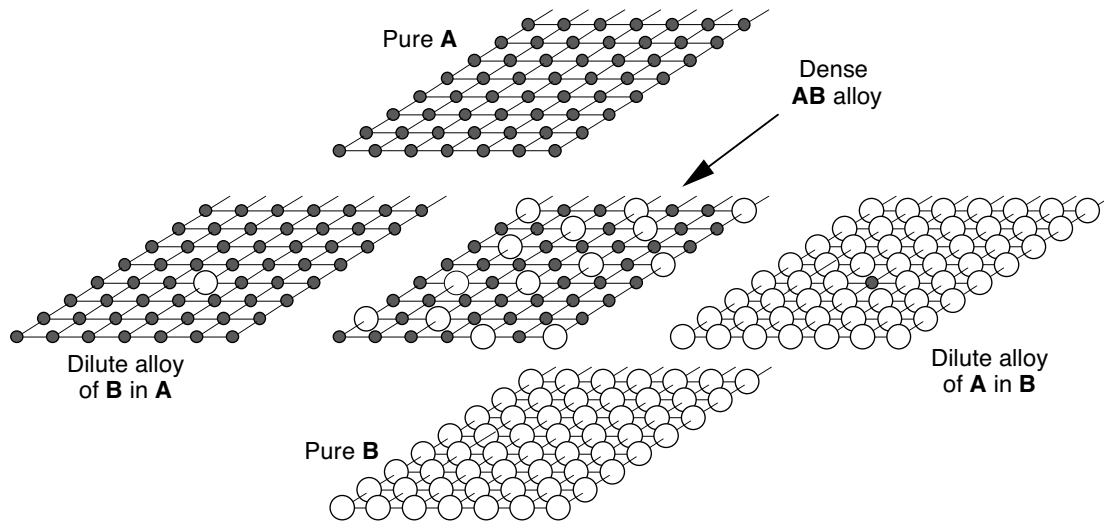


Figure 7.41 The resistivity at 300 K of silicon alloyed with small amounts phosphorus, both plotted on logarithmic axes. Alloying at this low level – the highest impurity concentration shown is just over one P atom for every 100 Si atoms – is generally referred to as *doping*. Notice that doping phosphorus dramatically reduces the resistivity of the silicon even at low levels. Notice also that even at its lowest value the resistivity is 100 times worse than that of typical metallic elements (Figure 7.34).

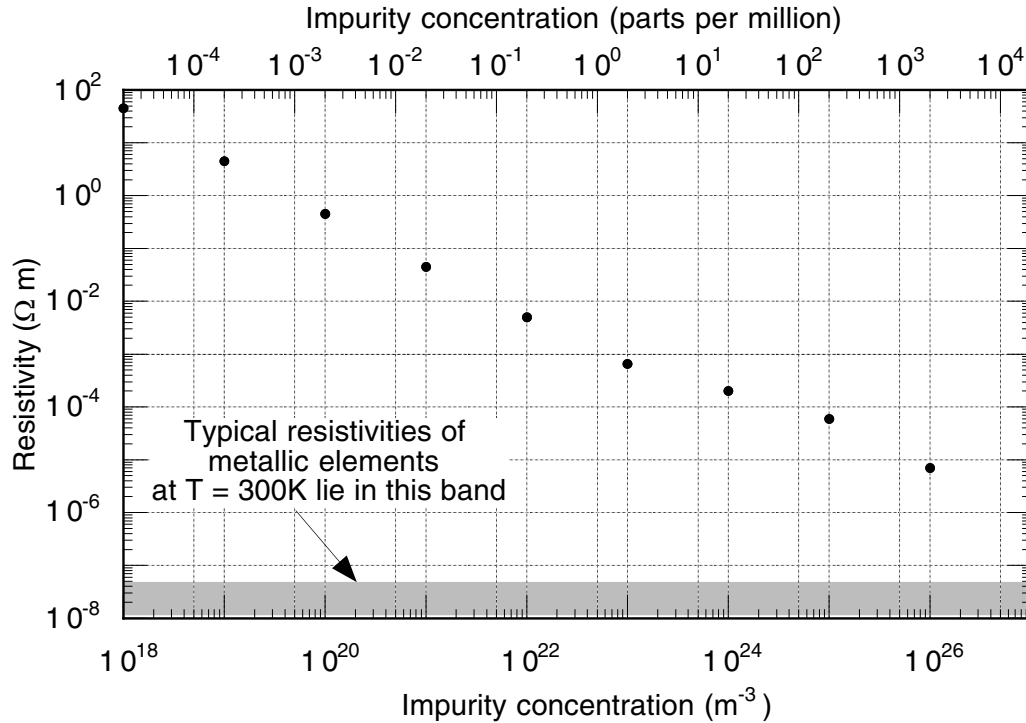


Figure 7.42 Calculation of the resistivity of relatively pure silicon plotted on a logarithmic scale versus temperature. Also shown for contrast is the resistivity of platinum also plotted on Figure 7.35. Note: The silicon data has been calculated from data tabulated in various sources. It should be taken as indicative of the trend of data only.

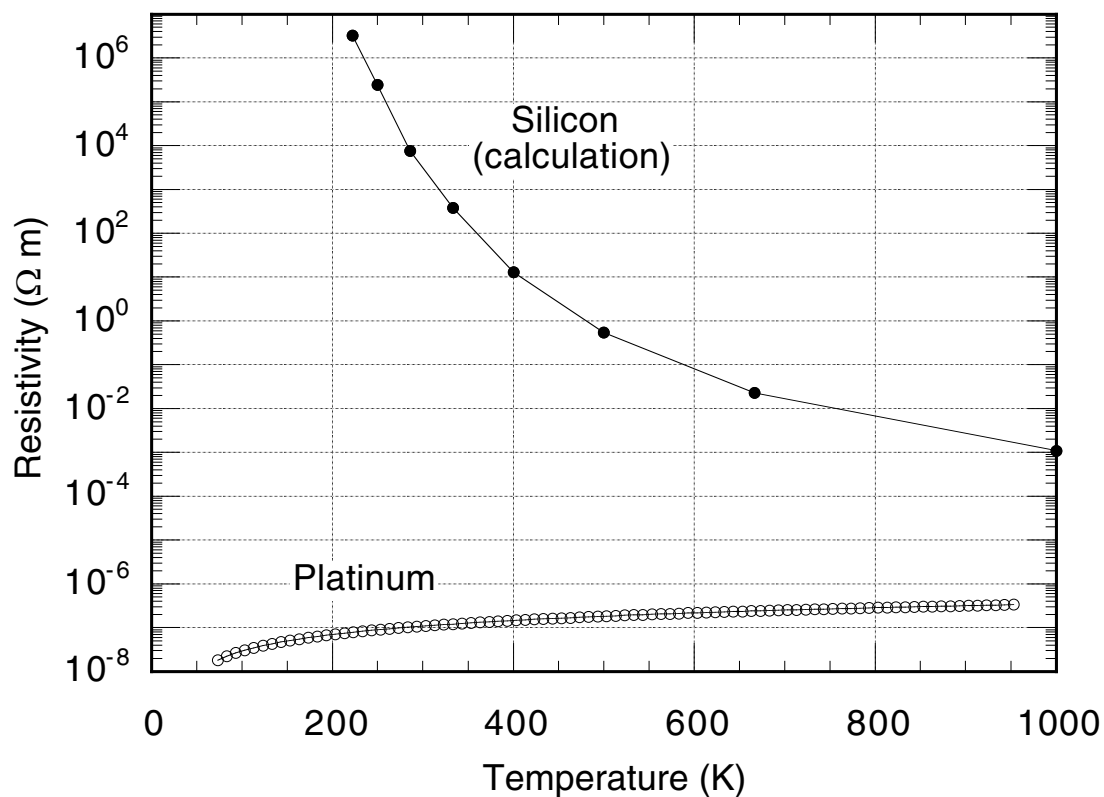


Figure 7.43 An illustration of the situation on an atom of semiconducting substance at $T = 0$ K. A low-energy quantum state is occupied, and a higher-energy quantum state is empty. The energy difference ΔE between the two states is very much greater than $k_B T$. The figure is drawn approximately to scale so that if ΔE is 1 eV, then $k_B T$ is $\approx 1/40$ eV, the value of $k_B T$ at around room temperature.

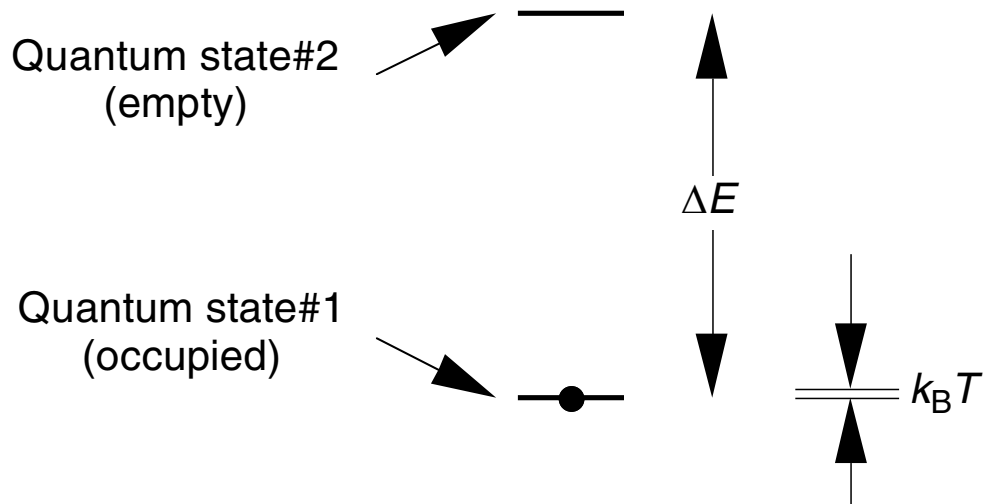


Figure 7.44 The situation of electrons within a semiconducting substance. (a) At $T = 0$ K the electrons occupy the lowest energy states, but (b) above $T = 0$ K a few higher energy states are populated. In (c) and (d) $T > 0$ K and an applied electric field causes electrons to move to neighbouring quantum states. Notice that field makes the electron in the upper state move one way, and the uncompensated positive charge in the lower quantum state move in the opposite direction.

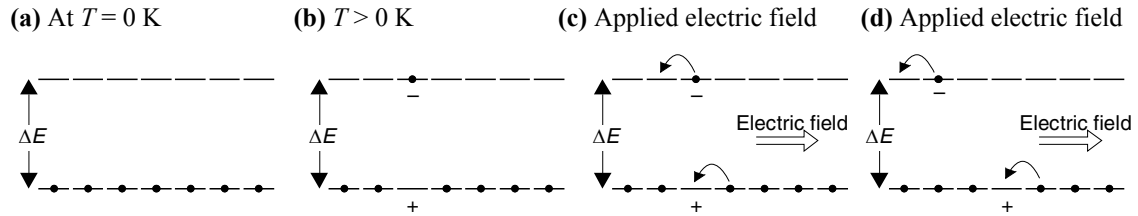
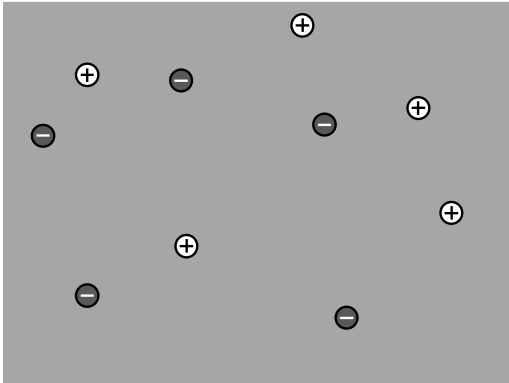


Figure 7.45. A region of a semiconductor with the lattice of atoms represented by a grey box. The number densities of hole and electron carriers are equal, and increase strongly with temperature. In fact the change in density with temperature is much more dramatic than figure indicates.

(a) Low temperature



(b) High temperature

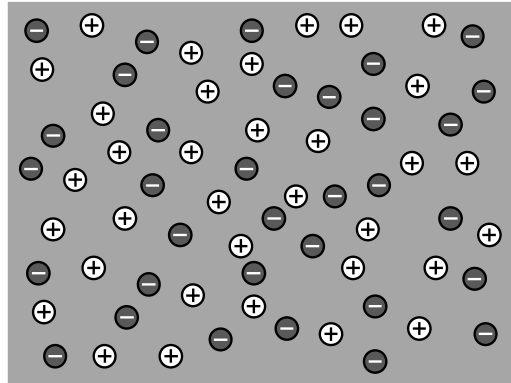


Figure 7.46 The mechanism by which a donor impurity causes an increase in the number of carriers available for conduction. (a) At $T = 0$ K, the extra electron on the phosphorus impurity is in a quantum state with an energy just below the conduction quantum states on neighbouring ions. The energy ΔE_d required to 'ionise' the impurity and place the donated electron into the conduction states is much less than the band gap ΔE . Thus at relatively low temperatures the electron leaves its localised quantum state and an electron carrier is created in the conduction band. (b) Notice that unlike the case of a carrier arising from processes intrinsic to the silicon, the electron carrier in the conduction states does not have a partner hole carrier in the valence states. There is however an immobile net positive charge left on the phosphorus impurity.

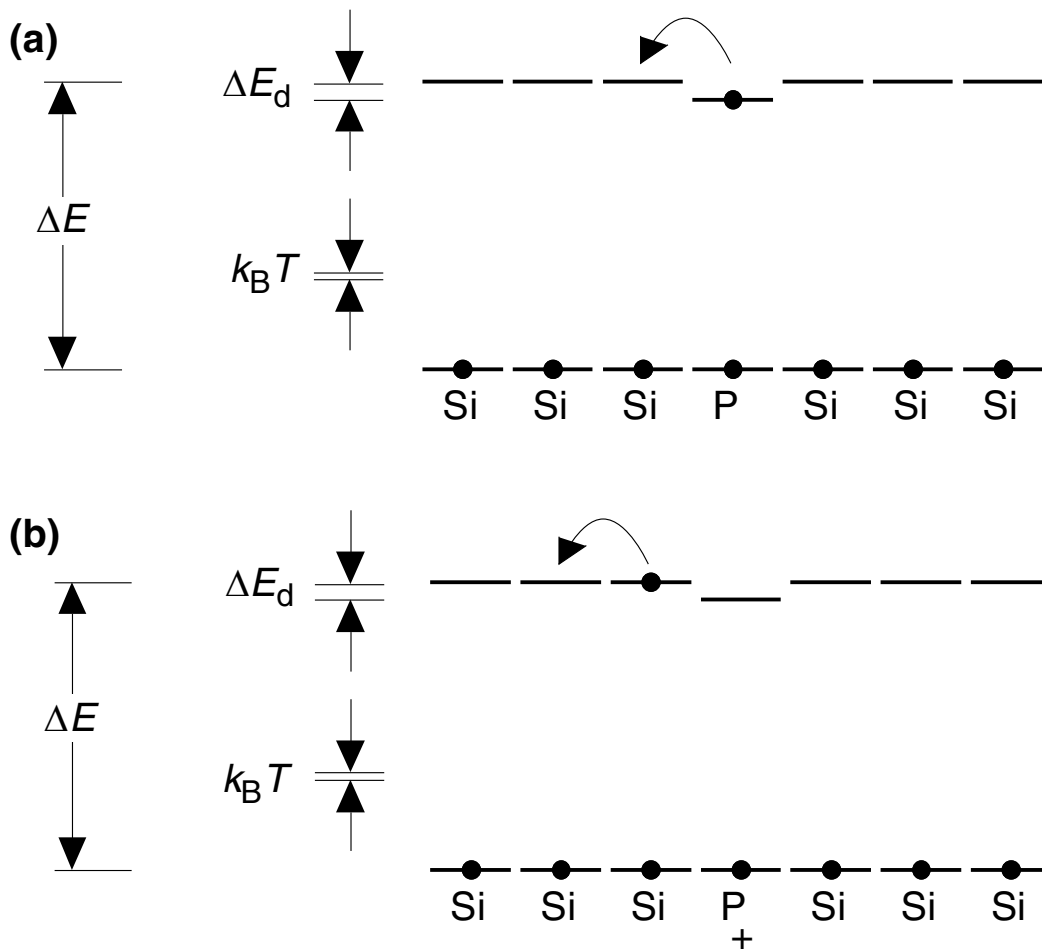


Figure 7.47 The mechanism by which an acceptor impurity causes an increase in the number of carriers available for conduction. (a) At $T = 0$ K, the quantum state on an aluminium equivalent to the valence state in silicon is unoccupied. The energy of this state is just above the valence quantum states on neighbouring ions. The energy ΔE_a required by an electron to occupy this quantum state is much less than the band gap ΔE . At relatively low temperatures, this capture can occur with high probability resulting in the creation of a hole carrier in the valence states of the silicon. (b) Notice that unlike the case of a carrier arising from processes intrinsic to the silicon, the hole carrier in the valence states does not have a partner electron carrier in the conduction states. There is however an immobile net negative charge left on the aluminium impurity.

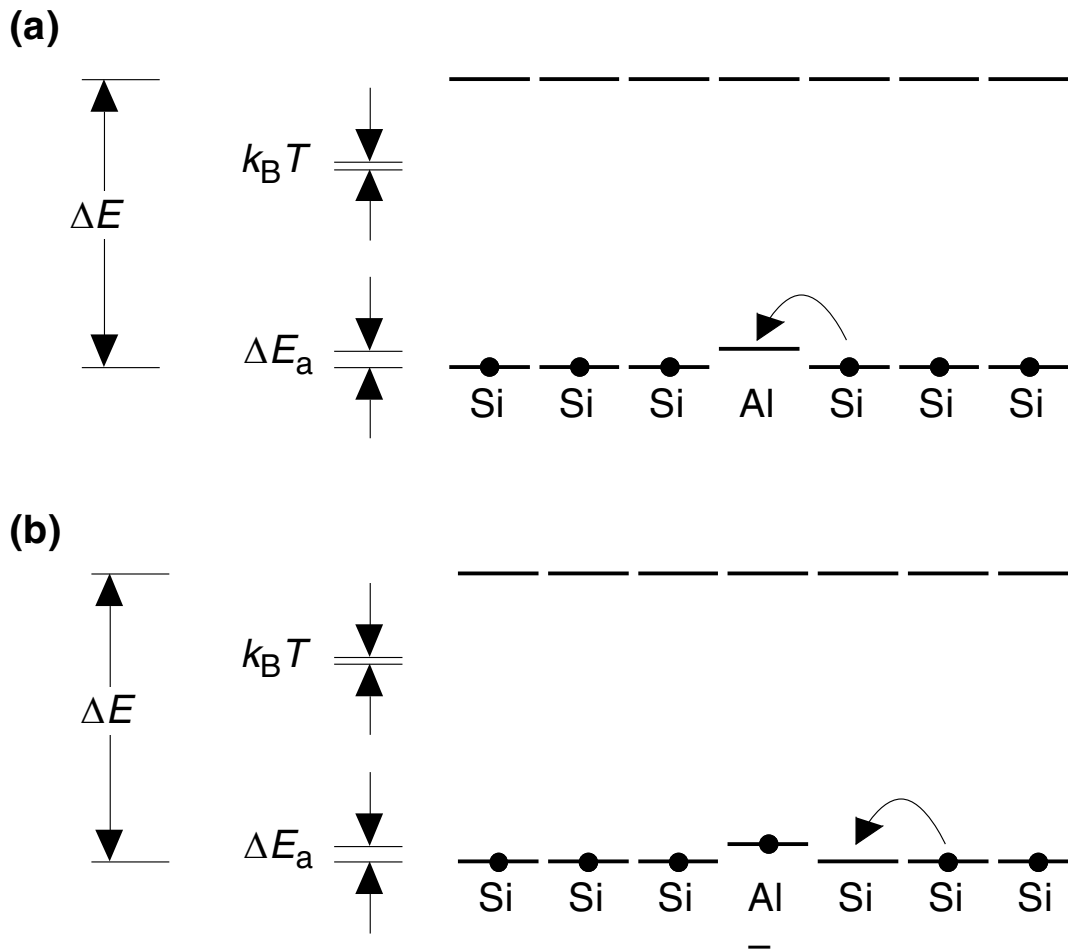


Figure 7.48 Selected data from Table 7.19 The upper graph shows the data for all the insulators and semiconductors in Table 7.16 with the exception of diamond. The thermal conductivity of diamond is so much greater than any other material that it distorts the scaling of the graph. The two unlabelled curves close to the temperature axis belong to tellurium and sulphur. The lower graph shows the data for a selection of metals. The vertical scale is the same as the upper graph showing that a typical value of the metallic conductivity is slightly greater for insulators. More striking is the different temperature dependence shown by metals and insulators. The metals show a less pronounced temperature dependence. In general the thermal conductivity appears to increase with decreasing temperature. However, two of the insulators show peaks in thermal conductivity as the temperature is lowered.

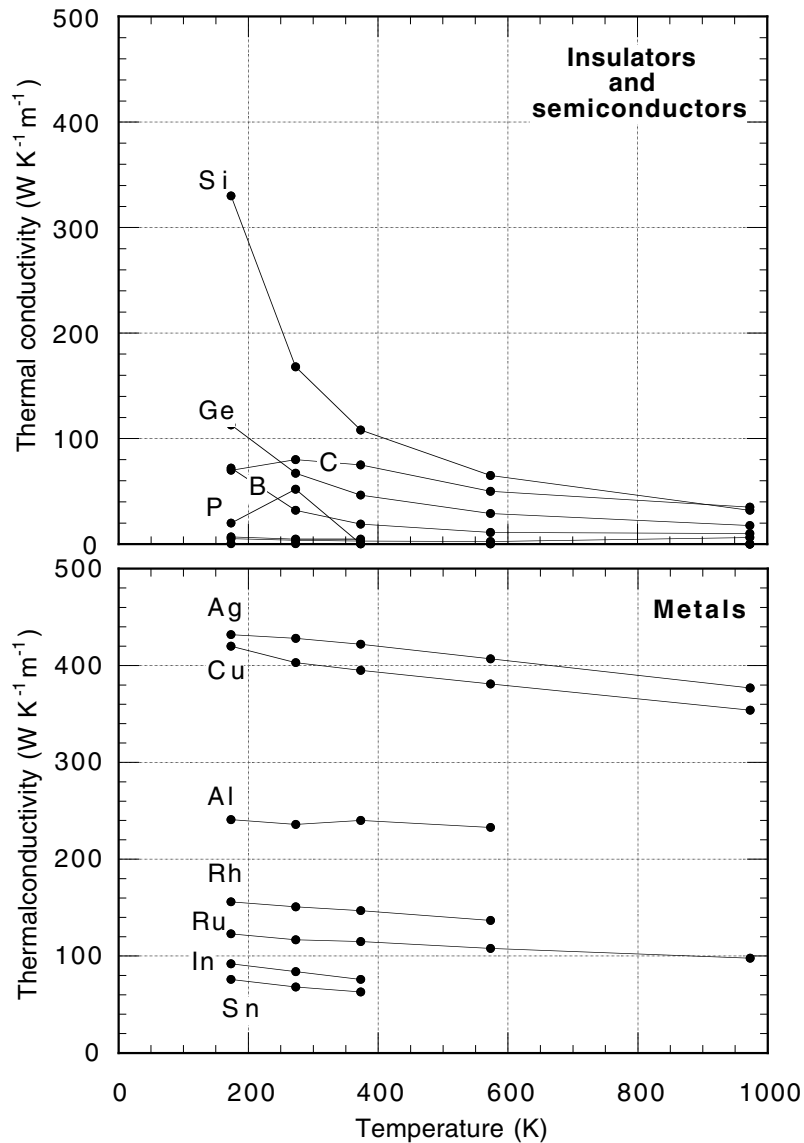


Figure 7.49 Simplified illustration of the calculation of thermal conductivity of ‘a gas’. This is the same as figure 5.20, but now we are applying it more generally to phonon and electron gases instead of just molecular gases.

The Figure shows three planes in ‘a gas’ perpendicular to a temperature gradient. The separation of the planes is λ_{mfp} , the mean free path of the particles. Thus particles that are travelling in the appropriate direction in either the top or the bottom plane will (probably) cross the central plane before colliding. Energy is carried across A in both directions, but *on average* more energy flows across A from the plane in the hotter region of the gas. The analysis of the thermal conductivity centres on the problem of evaluating the net energy flow across an area A .

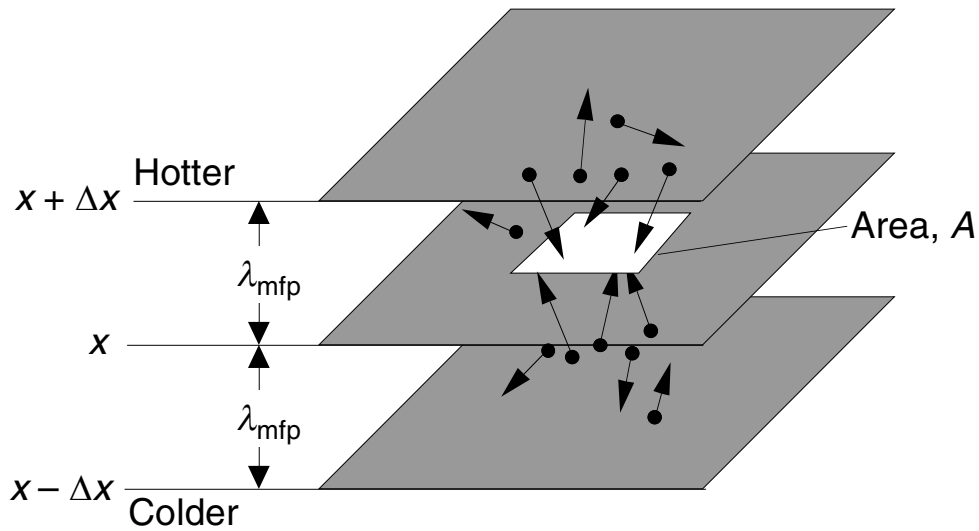


Figure 7.50 The refractive index of some optical glasses as a function of wavelength. The shaded region corresponds to the visible region of the spectrum. Longer wavelengths are described as infra-red, and shorter wavelengths as ultra-violet.

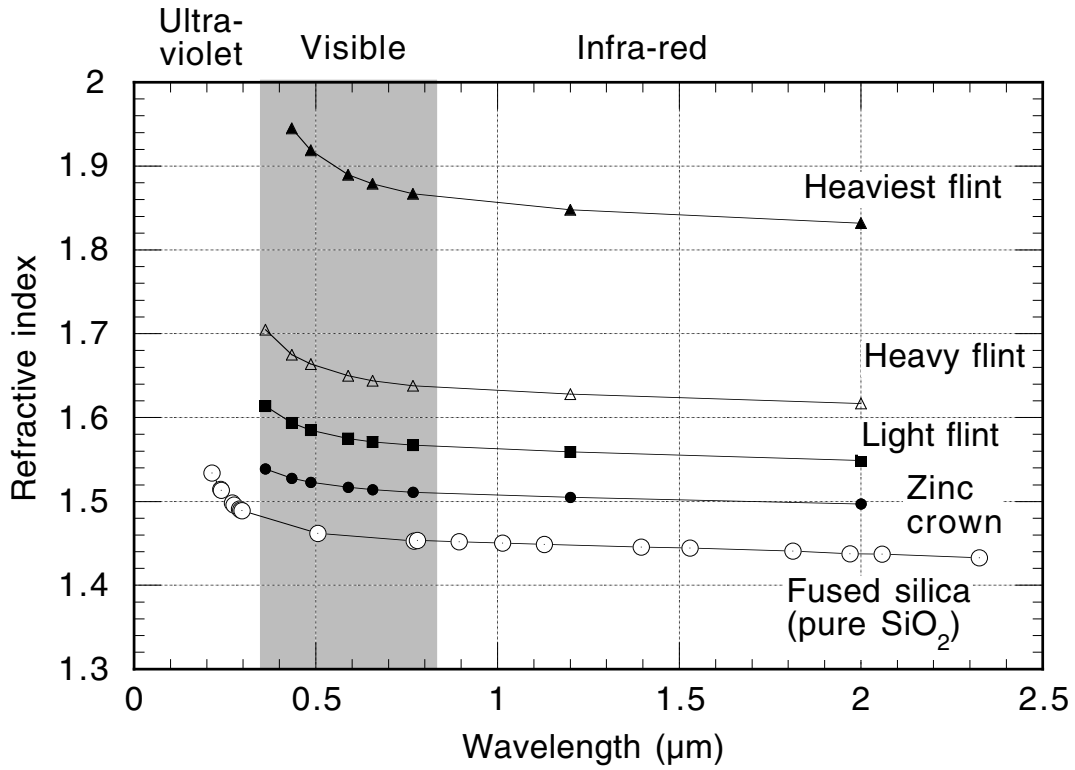
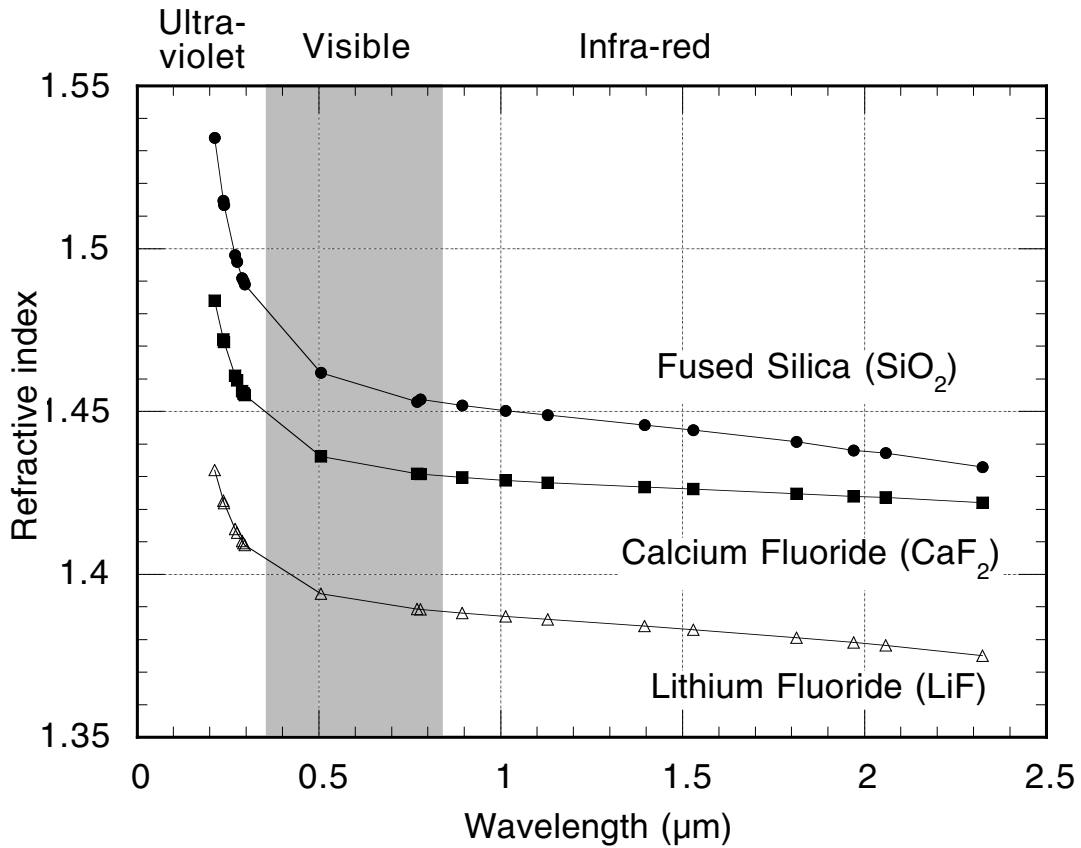
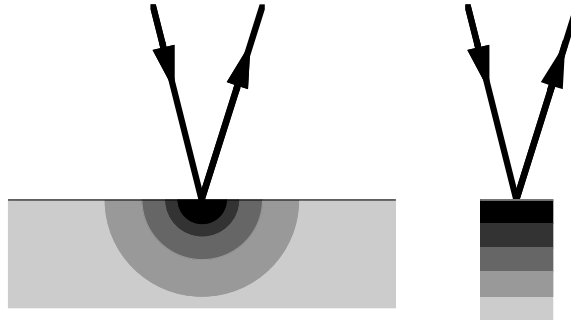


Figure 7.51 The refractive index of a three transparent insulators as a function of wavelength. The SiO_2 curve is also plotted on Figure 7.49 for comparison. The shaded region corresponds to the visible region of the spectrum. The longer wavelengths are therefore in the infra-red region of the spectrum, and the shorter wavelengths in the ultra-violet region.



From Example 7.22



From Example 7.23

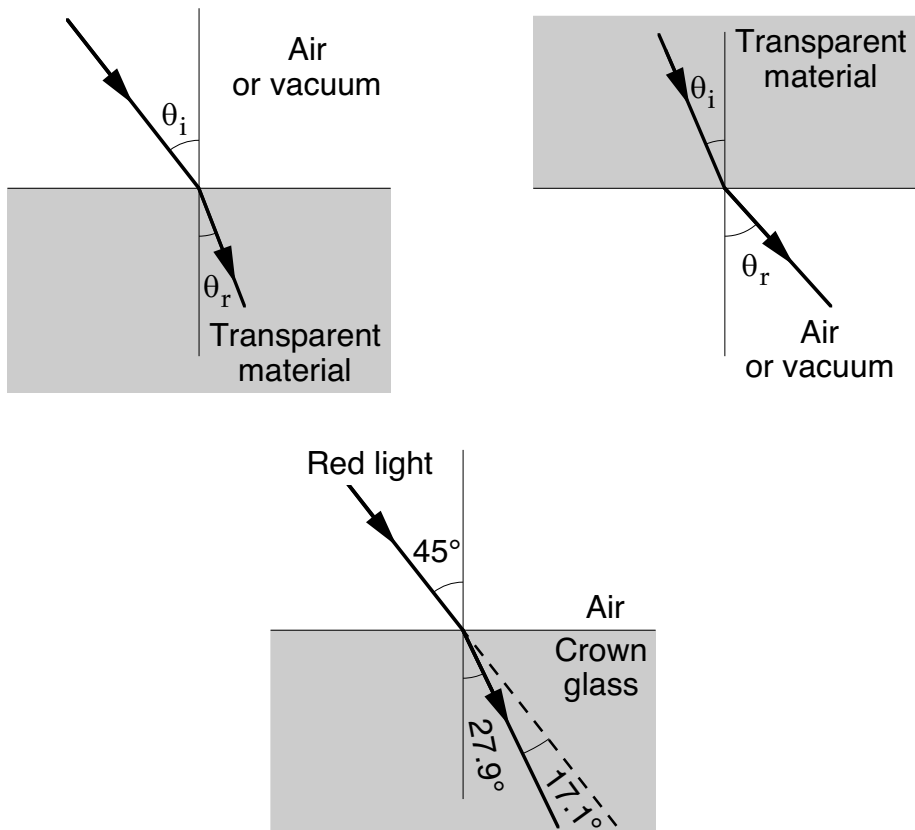


Figure 7.52 A simple model of the polarisation of an atom in an applied electric field. (a) The electron shells around an atom are much lower in mass than the nucleus. (b) & (c): When the direction of the applied electric field is reversed, the heavy nucleus moves much less than the charged electron shells.

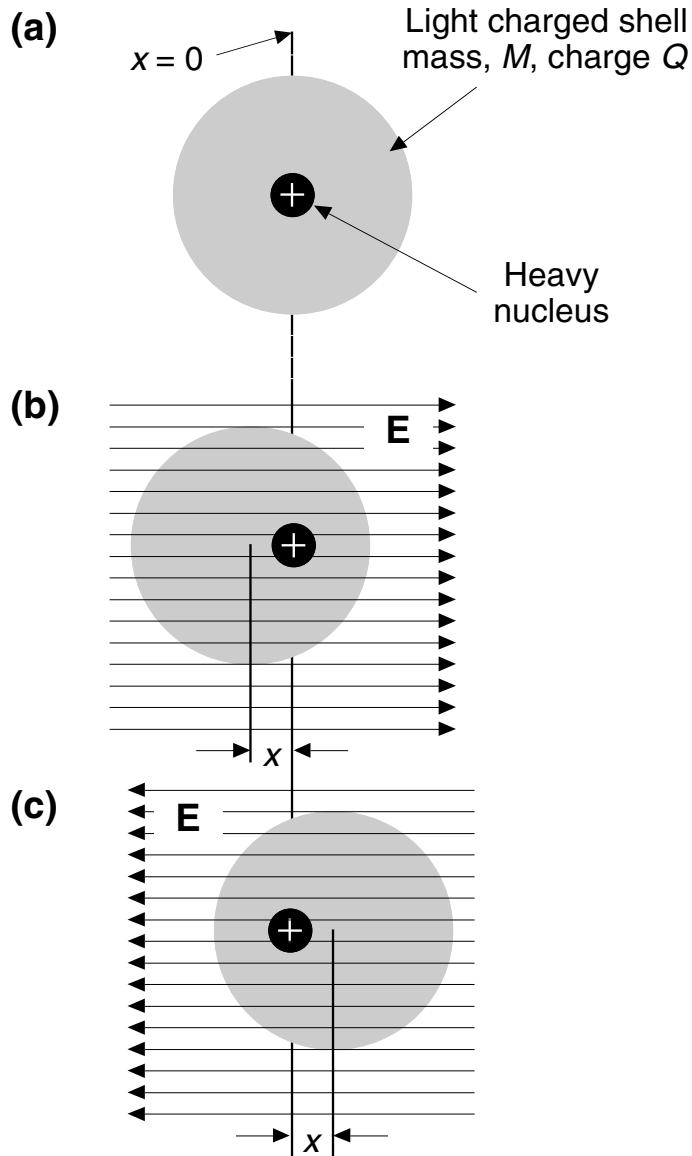


Figure 7.53 Classical and quantum mechanical description of resonance in a simple harmonic oscillator. (a) Classically, the amplitude of an oscillation grows dramatically when the oscillator is subject to a force at frequency $\omega = \omega_0 = \sqrt{K/M}$ (b) Quantum mechanically, when $\omega = \omega_0$ photons with energy $\hbar\omega$ are absorbed and the oscillator makes transitions between its quantum states.

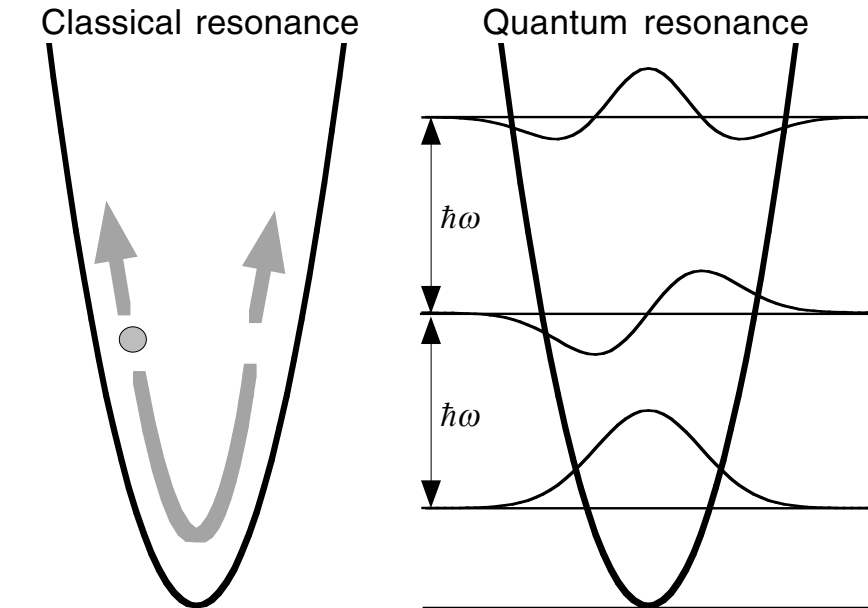


Figure 7.54 The data of Figure 7.50 re-plotted to show the refractive index of various glasses plotted as a function $1/\lambda^2$. The straight lines are least-squares fits to the data. The equations of the lines and the value of λ_0 inferred from the slope of the lines is given in the inset. In Example 7.24 we found that for $n_{\text{light}(\infty)} \approx 1.5$ implied $\lambda_0 \approx 0.167 \mu\text{m}$ whereas from this data we deduce $0.059 \mu\text{m}$. This factor 3 difference arises because in Example 7.24 we assumed just one electron per atom and used only an approximation for the electron density. However both analyses are simplified and *neither* should be trusted absolutely.

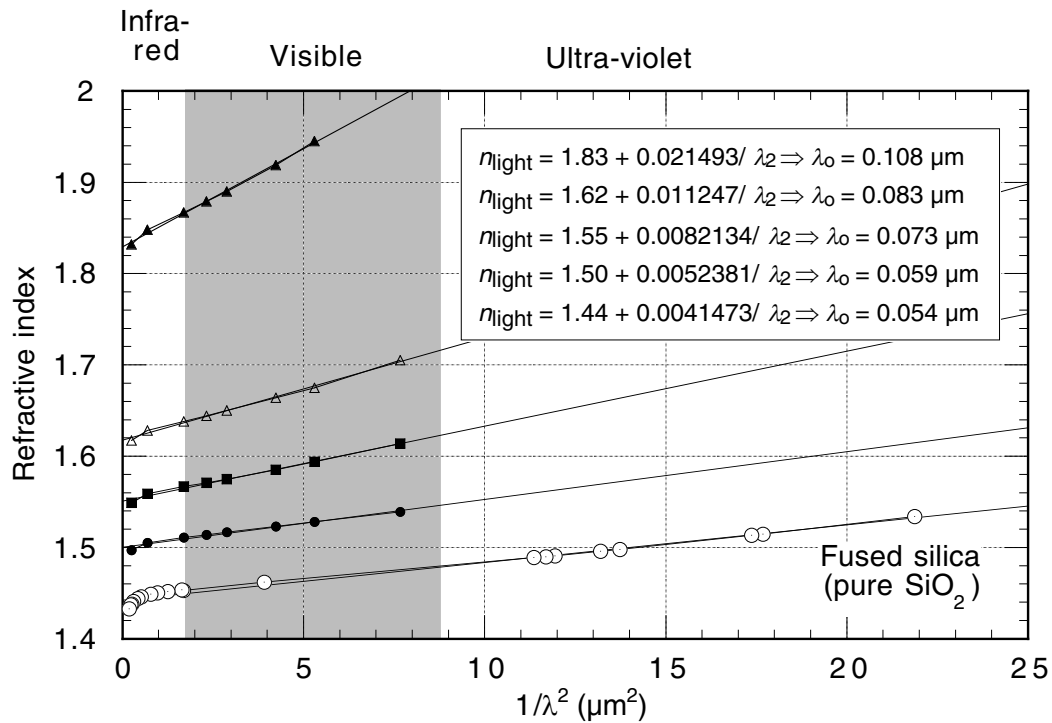


Figure 7.55 The processes underlying reflection of light from a metallic surface. (a) The incoming electromagnetic wave is strongly damped as it enters the metal. The length over which the field decays is known as the skin depth, δ , and is related to the conductivity, σ , of the metal as shown in Equation 7.155. (b) In the thin region, δ , in which the electric field is not zero, oscillating currents will flow. The currents are driven by the electric field of the light wave. (c) The oscillating currents re-radiate electromagnetic waves. Waves radiated into the solid are strongly absorbed, but waves radiated away from the surface can propagate easily.

(a) Incoming wave

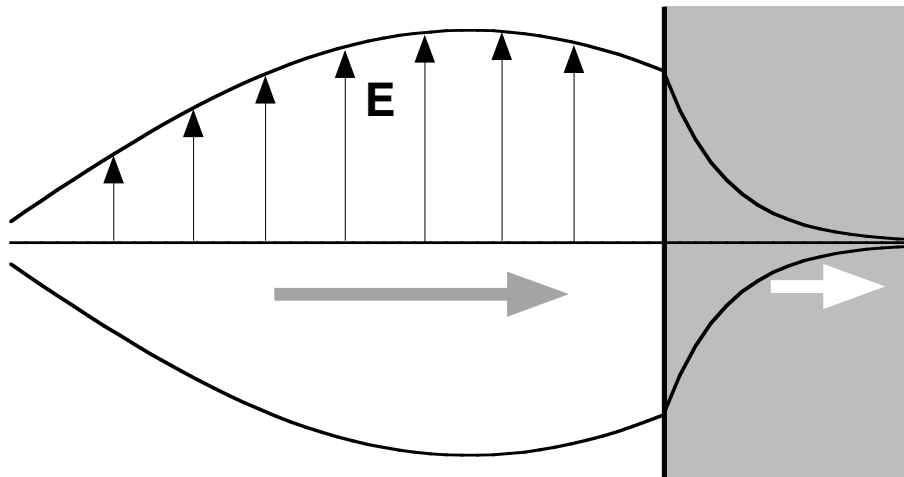


Figure 7.55 The processes underlying reflection of light from a metallic surface. (a) The incoming electromagnetic wave is strongly damped as it enters the metal. The length over which the field decays is known as the skin depth, δ , and is related to the conductivity, σ , of the metal as shown in Equation 7.155. (b) In the thin region, δ , in which the electric field is not zero, oscillating currents will flow. The currents are driven by the electric field of the light wave. (c) The oscillating currents re-radiate electromagnetic waves. Waves radiated into the solid are strongly absorbed, but waves radiated away from the surface can propagate easily.

(b) Charge oscillations due to incoming wave (a)



Figure 7.55 The processes underlying reflection of light from a metallic surface. (a) The incoming electromagnetic wave is strongly damped as it enters the metal. The length over which the field decays is known as the skin depth, δ , and is related to the conductivity, σ , of the metal as shown in Equation 7.155. (b) In the thin region, δ , in which the electric field is not zero, oscillating currents will flow. The currents are driven by the electric field of the light wave. (c) The oscillating currents re-radiate electromagnetic waves. Waves radiated into the solid are strongly absorbed, but waves radiated away from the surface can propagate easily.

(c) Re-radiated (reflected) wave due to the charge oscillations (b)

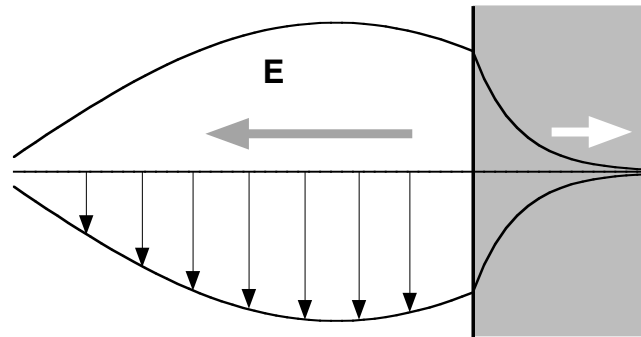
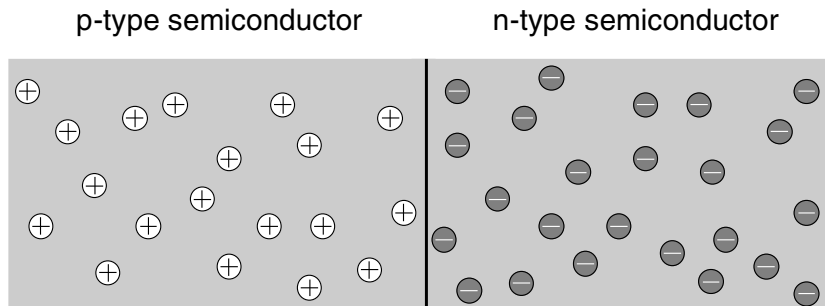


Figure 7.56 Illustration of the use of a semiconductor pn junction as a photodiode and light emitting diode (LED). (a) How we imagine the arrangement of carriers at the moment a pn junction is formed. (b) The arrangement a short while later. The carriers have diffused a short distance across the junction and annihilated the ‘native’ carriers. This leaves uncompensated donor and acceptor charges in the so-called *depletion layer*. (c) When used as an LED, an electric current across junction injects holes and electrons into the depletion layer where they annihilate. (d) When used as a photodiode light with photon energy greater than the energy gap can create hole–electron pairs. If these are created in the depletion layer they are pulled apart by the built in electric field and give rise to a current.

(a) pn junction at the moment of formation



(b) Depletion layer

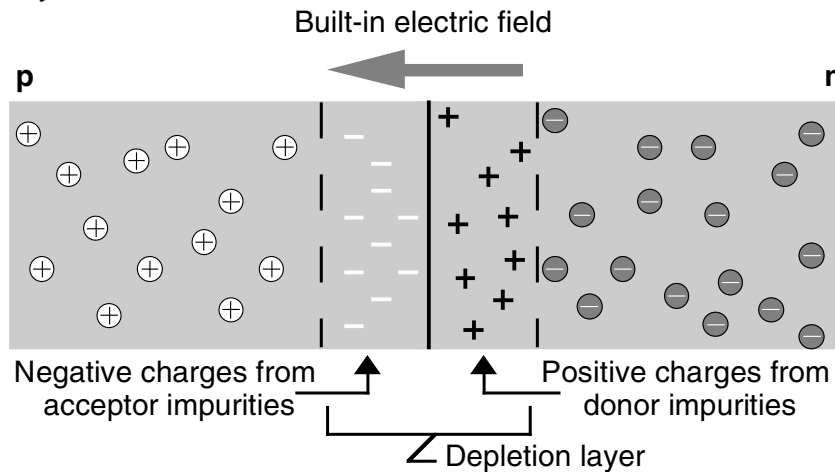
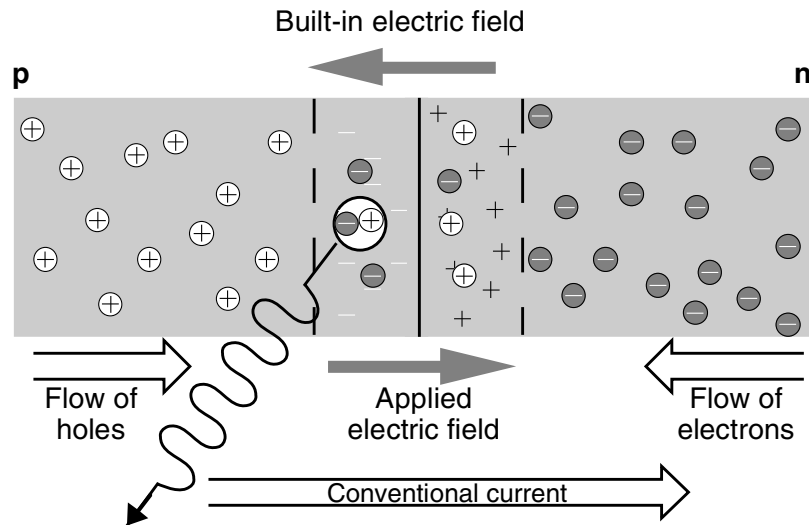


Figure 7.56 Illustration of the use of a semiconductor pn junction as a photodiode and light emitting diode (LED). (a) How we imagine the arrangement of carriers at the moment a pn junction is formed. (b) The arrangement a short while later. The carriers have diffused a short distance across the junction and annihilated the 'native' carriers. This leaves uncompensated donor and acceptor charges in the so-called *depletion layer*. (c) When used as an LED, an electric current across junction injects holes and electrons into the depletion layer where they annihilate. (d) When used as a photodiode light with photon energy greater than the energy gap can create hole–electron pairs. If these are created in the depletion layer they are pulled apart by the built in electric field and give rise to a current.

(c) Light-emitting diode



(d) Photodiode

